
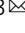








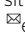


Distinct and additive effects of calorie restriction and rapamycin in aging skeletal muscle

Daniel J. Ham ^{1,3}, Anastasiya Börsch^{1,3}, Kathrin Chojnowska¹, Shuo Lin¹, Aurel B. Leuchtman ¹, Alexander S. Ham¹, Marco Thürkauf¹, Julien Delezie¹, Regula Furrer¹, Dominik Burri ¹, Michael Sinnreich², Christoph Handschin ¹, Lionel A. Tintignac², Mihaela Zavolan ^{1,3}, Nitish Mittal ^{1,3} & Markus A. Rüegg ^{1,3}

Preserving skeletal muscle function is essential to maintain life quality at high age. Calorie restriction (CR) potentially extends health and lifespan, but is largely unachievable in humans, making “CR mimetics” of great interest. CR targets nutrient-sensing pathways centering on mTORC1. The mTORC1 inhibitor, rapamycin, is considered a potential CR mimetic and is proven to counteract age-related muscle loss. Therefore, we tested whether rapamycin acts via similar mechanisms as CR to slow muscle aging. Here we show that long-term CR and rapamycin unexpectedly display distinct gene expression profiles in geriatric mouse skeletal muscle, despite both benefiting aging muscles. Furthermore, CR improves muscle integrity in mice with nutrient-insensitive, sustained muscle mTORC1 activity and rapamycin provides additive benefits to CR in naturally aging mouse muscles. We conclude that rapamycin and CR exert distinct, compounding effects in aging skeletal muscle, thus opening the possibility of parallel interventions to counteract muscle aging.

¹Biozentrum, University of Basel, Basel, Switzerland. ²Department of Biomedicine, Pharmazentrum, University of Basel, Basel, Switzerland. ³These authors contributed equally: Daniel J. Ham, Anastasiya Börsch, Mihaela Zavolan, Nitish Mittal, Markus A. Rüegg. email: dan.ham@unibas.ch; nitish.mittal@unibas.ch; markus-a.ruegg@unibas.ch

Dietary or calorie restriction (CR) is the most potent and reproducible intervention to extend lifespan. However, CR as a human lifestyle is considered largely unachievable based on the sheer willpower required to maintain a low-calorie diet along with potential side effects including extreme leanness and cold sensitivity¹. In order to eventually translate the health benefits of CR into medical treatments for aging humans, a mechanistic understanding of how CR confers longevity is essential². CR, along with many of the interventions known to prolong lifespan, dampen the activity of nutrient-sensing pathways, which center around the mammalian target of rapamycin complex 1 (mTORC1), thereby alleviating protein synthetic burden and promoting intrinsic quality control processes, like autophagy³. Findings that the mTORC1 inhibitor, rapamycin (RM), extends lifespan in yeast⁴, flies⁵, worms⁶ and mice⁷ strengthened the hypothesis that mTORC1 inhibition is fundamental to CR-induced lifespan extension⁸.

Over the past century, global life expectancy has nearly doubled, but, as the World Health Organization recognized while declaring 2021–2030 the decade of healthy aging: “adding more years to life can be a mixed blessing if it is not accompanied by adding more life to years”⁹. A well-functioning neuromuscular system is fundamental to ensure more life comes with more years. Since anabolic pathways, especially those involving mTORC1, promote both muscle growth^{10,11} and sarcopenia, the age-related loss of muscle mass¹², skeletal muscle is considered a potential sticking point for achieving both life extension and life quality via CR and RM. However, we have recently demonstrated that long-term RM treatment is overwhelmingly, although not entirely, beneficial for aging mouse skeletal muscle¹³. While a thorough examination of whether long-term CR, spanning the time of sarcopenic development (20–28 months in mice¹⁴) counteracts phenotypic and molecular signatures of sarcopenia is still lacking, life-long CR appears to afford similar benefits as RM to aging skeletal muscle, including a more stable neuromuscular junction¹⁵ and slower age-related muscle loss^{16,17}. Could RM, therefore, function as a CR mimetic to slow muscle aging?

Studies in mice highlight that although both CR and RM blunt mTORC1 activity and promote autophagy^{18,19}, their effects on insulin signaling strongly diverge, with CR improving and RM impairing glucose tolerance^{19,20}. Similarly, molecular profiling studies in mouse liver have shown that the vast majority of acute transcriptomic, metabolomic²¹ and proteomic responses to CR and RM are distinct²². But is this a case of ‘all roads lead to Rome’, where CR and RM travel different paths to mTORC1 suppression, or do these two quintessential life-prolonging interventions travel different roads with distinct destinations? If the former is true, we reasoned that (1) the molecular and phenotypic signatures of long-term CR and RM in skeletal muscle should overlap; (2) the beneficial effects of CR should be lost if skeletal muscle mTORC1 activity remains high and; (3) the effects of RM should be lost in calorie-restricted mice.

Using repeated measurements of whole-body muscle function and body composition, multi-muscle gene expression profiling and extensive endpoint examination of isolated muscle function and fiber-type properties, we first thoroughly characterized the impact of long-term CR starting from 15 or 20 months until 30 months of age, thus covering the period when sarcopenia develops. Compared to a weight-controlled, ad libitum-fed control group, CR mice improved whole-body and isolated relative muscle function and experienced a fast-to-slow shift in muscle fiber phenotype. While much of this phenotype was shared by RM-treated mice¹³, gene expression signatures of CR and RM were strikingly divergent, the only exception relating to the suppression of age-related increases in immune and inflammatory responses. In further opposition to overlapping functions,

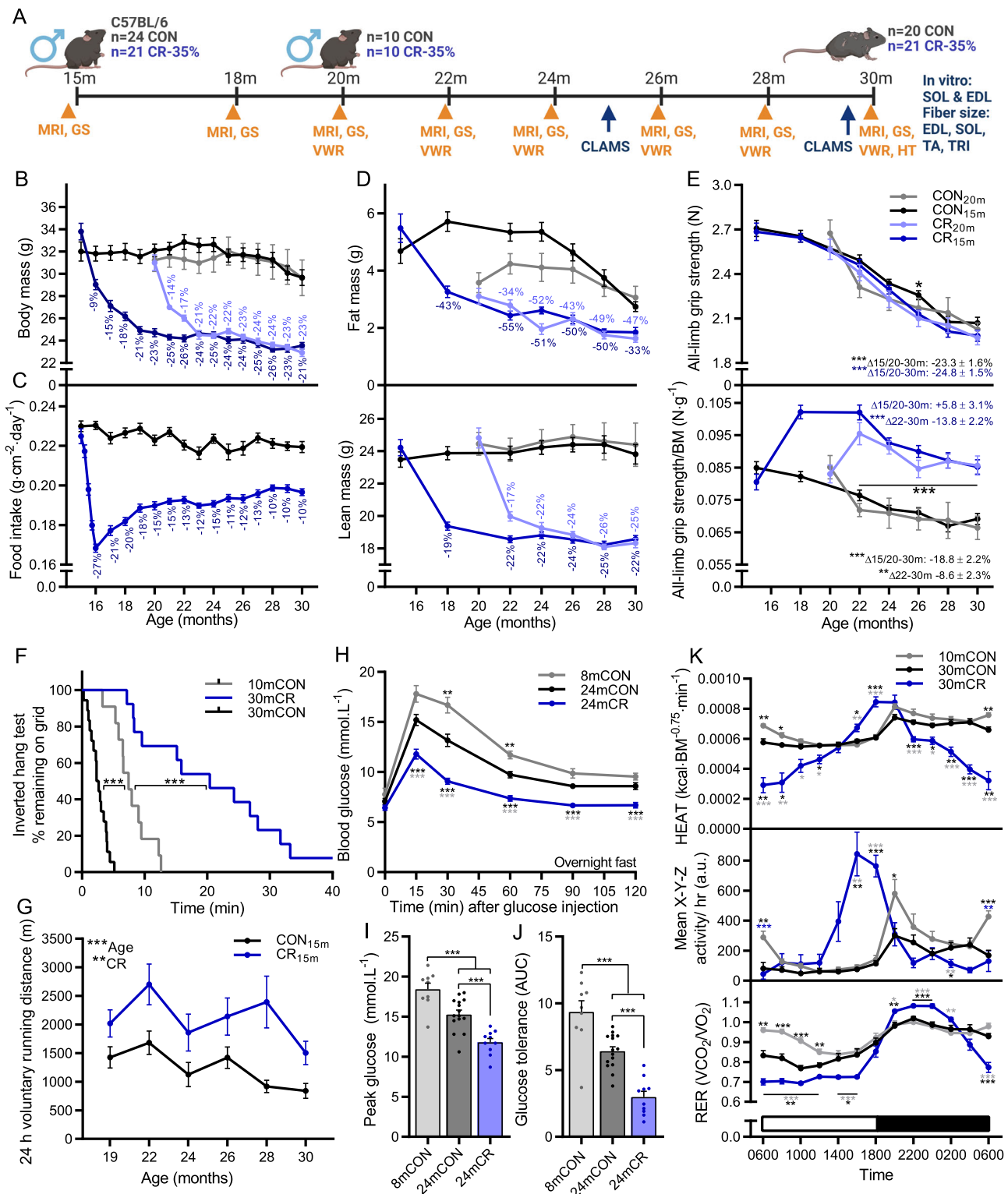
CR improved markers of muscle quality, including autophagy blockade as seen by p62 build up, plasma creatine kinase (CK) levels, centro-nucleated fibers and in vitro muscle function in a nutrient-insensitive, mTORC1-driven model of premature muscle aging, without suppressing mTORC1 activity. Most conclusively, long-term RM treatment effectively counteracted skeletal muscle aging in both ad libitum-fed and CR mice. We therefore demonstrate that RM and CR exert distinct and frequently additive effects on aging skeletal muscle, thereby opening the possibility of parallel interventions to counteract aging.

Results

Adaptations to calorie restriction favor whole-body muscle function but do not prevent an age-related decline. After habituation to single housing and the AIN-93M diet, 15- (CR_{15m}) or 20- (CR_{20m}) month-old male mice underwent a weekly, stepwise reduction in food intake from 100% (3.2 g) to 90% (2.9 g), 80% (2.6 g), 70% (2.3 g) and finally 65% (2.1 g) of ad libitum levels until 30 months of age (Fig. 1A). After the initial month, calorie restricted mice continued to rapidly lose body mass for 2–3 months and then maintained a body mass between 21 and 26% below control mice from ~19 or 23 months to 30 months for CR_{15m} and CR_{20m} groups, respectively (Fig. 1B). Food intake normalized to body surface area indicated that calorie restricted mice do not fully compensate for reduced food intake through body mass reductions, partially adapting to the low-energy environment through energy sparing processes (Fig. 1C). After initially drawing on energy reserves, particularly fat²³, calorie restricted mice display a range of adaptations to cope with the shortfall in energy intake, including improving energy absorption, reducing non-essential organ mass and lowering body temperature and energy expenditure²⁴. Compared to controls, 24-month-old calorie restricted mice had larger proportional differences in fat mass than lean mass, but smaller absolute differences (Fig. 1D). A progressive, age-related loss of whole-body fat mass in control mice narrowed the difference in fat, but not lean mass between CR and CON mice at 30 months of age.

Repeated all-limb grip strength measures spanning the treatment period show that the progressive age-related loss of absolute grip strength was similar in both control and calorie restricted mice ($P < 0.001$; Fig. 1E, upper). However, due to the initial rapid loss of body mass, calorie restricted mice strongly increased relative grip strength ($N \cdot g \text{ body mass}^{-1}$) over the initial 2–3 months before displaying a similar age-related decline in relative grip strength as control mice from 22 to 30 months (Fig. 1E, lower). As such, compared to the initial recording (15 or 20 months), relative grip strength significantly declined across the treatment period in control mice ($P < 0.001$), but not in CR mice. However, when compared to the 22-month recording, the decline in relative grip strength was not different between control ($P < 0.002$) and calorie restricted ($P < 0.001$) mice at 30 months. Consistent with improved relative strength, calorie restriction potently improved inverted grid-hang time compared to both 10mCON and 30mCON groups (Fig. 1F; $P < 0.001$). Similarly, voluntary running activity over a 24 h period was consistently improved in calorie restricted mice across the trial (Fig. 1G; $P < 0.01$).

After an overnight fast for all groups, calorie restricted mice showed a marked increase in glucose tolerance and significantly lower blood glucose levels than 8 and 24-month-old control mice at each point after glucose injection (Fig. 1H). CR also lowered peak glucose (Fig. 1I) and the area under the curve (AUC; Fig. 1J). Despite similar body mass and whole-body fat mass, 24-month-old control mice showed lower blood glucose at 30 and 60 min after glucose injection as well as a lower peak glucose and AUC



than 8-month-old control mice. Similarly, improvements in glucose tolerance have been observed between 20 and 28 months of age in wild type mice²⁵ and also in mice genetically modified to have high muscle fiber mTORC1 activity²⁶, a commonly observed feature of sarcopenic muscle^{13,27–29}.

While daylight regulated whole-body metabolism in control mice; with energy expenditure, activity and RER all high at night and low during the day; metabolism in CR mice centered around food availability (Fig. 1K and Supplementary Fig. 1A–F). In CR

mice, energy expenditure (Fig. 1K upper) and activity (Fig. 1K middle) were tightly restricted to the hours immediately before and immediately after their 5 pm food allocation. Despite displaying characteristic anticipatory increases in activity and energy expenditure prior to food, RER remained at around 0.7 (Fig. 1K lower), indicating almost exclusive fat utilization, before a food- and therefore glucose availability-related increase during night-time hours. In line with lower food intake per body surface area in CR mice (Fig. 1C), mean energy expenditure per body

Fig. 1 CR promotes beneficial metabolic and functional adaptations but does not prevent the age-related loss of muscle function. **A** Experimental design schematic showing start and endpoints of middle and late intervention groups as well as time course of physiological measures, including body composition (MRI), grip strength (GS), voluntary wheel running (VWR), whole-body metabolism (CLAMS), hang test (HT) and glucose tolerance test (GTT). **B** Body mass for mouse groups fed ad libitum or 65% of ad libitum beginning at 15 months (CON_{15m} and CR_{15m}) or 20 months (CON_{20m} and CR_{20m}) of age; $n = 18$ (CON_{15m}), 13 (CR_{15m}), 5 (CON_{20m}) and 8 (CR_{20m}). **C** Mean daily food intake normalized to body surface area for middle-aged groups; $n = 18$ (CON_{15m}) and 13 (CR_{15m}). **D** Bimonthly recordings of whole-body fat (upper) and lean mass (lower); $n = 18$ (CON_{15m}), 13 (CR_{15m}), 6 (CON_{20m}), and 8 (CR_{20m}) mice. **E** absolute (upper) and body mass normalized (lower) all-limb grip strength; $n = 19$ (CON_{15m}), 14 (CR_{15m}), 6 (CON_{20m}), and 8 (CR_{20m}) mice. **F** Kaplan-Meier plot for the inverted grid-hang test performed prior to endpoint measures at 30 months of age for the middle-aged group; $n = 11$ (10mCON), 18 (CON_{15m}), and 13 (CR_{15m}) mice. **G** Twenty-four hours of voluntary running-wheel distance; $n = 16$ (CON_{15m}), 13 (CR_{15m}), 6 (CON_{20m}), and 9 (CR_{20m}) mice. Glucose tolerance test parameters including **H** blood glucose response to 2 mg·kg⁻¹ glucose injection (I.P.), **I** peak glucose and **J** area under the curve/glucose tolerance; $n = 15$ (24mCON), 10 (24mCR) and 9 (8mCON). **K** Whole-body metabolic analysis of energy expenditure normalized to body surface area (upper), mean X-Y-Z activity (middle) and respiratory exchange ratio (VCO₂/VO₂; lower) reported every 2 h across one full day (white)/night (black) cycle in the month prior to endpoint measures; $n = 12$ (10mCON), 9 (30mCON), and 7 (30mCR) mice. Data are presented as mean ± SEM. Two-way repeated-measures ANOVA with Tukey post hoc tests (**B-E**, **G**, **H**, **K**), Mantel-Cox log rank (**F**), and one-way ANOVA with Fisher's LSD post hoc tests (**I**, **J**) was used to compare the data. *, **, and *** denote a significant difference between groups of $P < 0.05$, $P < 0.01$, and $P < 0.001$, respectively. Colored asterisks refer to the group of comparison. Experimental scheme in **A** created with BioRender.com.

surface area was -8.8 and -8.5% lower ($P < 0.05$) during day-time hours and -16.6% and -21.0% lower during night-time hours at 25 and 30 months of age in CR than control mice (Supplementary Fig. 1C). Together, these data indicate that calorie restricted mice shed excess tissue mass and induce metabolic adaptations to minimize energy use and maximize energy uptake when scarce food becomes available. Since the extent of metabolic adaptations and lifespan extension increase in parallel with that of calorie restriction, these adaptations are thought to be central to the health and longevity benefits of CR^{24,30}. While these changes initially lead to a substantial increase in relative grip strength, calorie restricted mice also display a progressive age-related loss of grip strength indicating that while CR clearly improves muscle functional parameters, mice are not entirely spared from muscle aging.

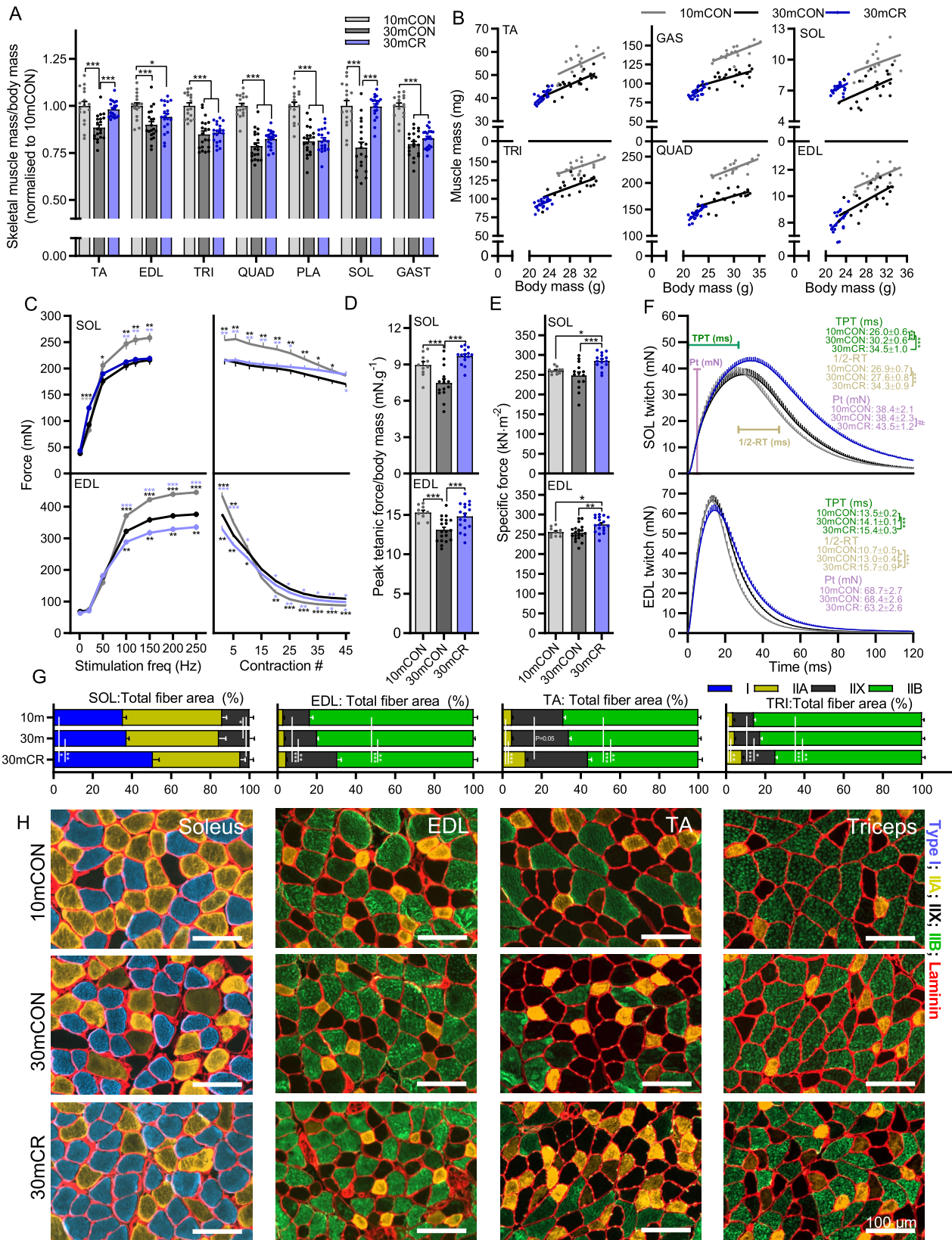
Calorie restriction promotes a fast-to-slow muscle phenotype transition. Aging reduced absolute (Supplementary Fig. S1G) and relative (mg/g body mass) mass (Fig. 2A) in all measured muscles. CR further reduced absolute muscle mass in the fast-twitch *tibialis anterior* (TA), *extensor digitorum longus* (EDL), *triceps brachii* (TRI), *quadriceps* (QUAD), *plantaris* (PLA) and *gastrocnemius* (GAS) muscles but not in the slow-twitch *soleus* (SOL) muscle (Supplementary Fig. 1G). When accounting for body mass, muscle mass was similar in 30mCON and 30mCR groups for all fast-twitch muscles, except TA, which along with the slow-twitch SOL muscle were significantly heavier relative to body mass in 30mCR than 30mCON mice (Fig. 2A). While correlation graphs indicate that the muscle-to-body mass ratio was similar for all fast twitch muscles, SOL mass was clearly higher for a similar body mass in 30mCR than 30mCON mice (Fig. 2B). In line with measures of body composition, CR reduced the absolute mass of all major organs (heart, spleen, kidney, liver) as well as epididymal white and interscapular brown fat depositions and prevented the age-related accumulation of non-functional mass (i.e., seminal vesicles; Supplementary Fig. 1H). Proportional to body mass, CR preserved heart, liver, and brown fat mass while shedding white fat, kidney, and spleen mass (Supplementary Fig. 1I).

Preferential sparing of slow-twitch muscle was also observed in measures of isolated muscle function in the fast EDL and slow SOL muscle (Fig. 2C–F). Long-term CR did not alter the strong age-related reduction in absolute tetanic force in the SOL but further lowered tetanic force in EDL muscle from 100–250 Hz (Fig. 2C, left). In response to repeated stimulations, tetanic force dropped more rapidly in the 10mCON group than either 30mCON or 30mCR groups (Fig. 2C, right). Despite producing significantly greater absolute force at the start of the assay in both

SOL and EDL, force in the 10mCON was not different to the other groups after 45 contractions in SOL and significantly lower than both other groups after 20 contractions in the EDL (Fig. 2C, right). After 45 contractions, 30mCR mice produced significantly more force than 30mCON mice in SOL muscle, but less in EDL muscle. In line with body mass-normalized grip strength measurements, calorie restriction completely prevented the age-related loss of SOL and EDL peak tetanic force (Fig. 2D). This was at least partially the result of improved muscle quality in 30mCR mice, which showed significantly higher specific muscle force, representing peak force normalized to muscle cross-sectional area, in both SOL and EDL muscle (Fig. 2E). Aging slowed muscle twitch properties with significantly longer time-to-peak tension in SOL and a longer half-relaxation time in the EDL muscle (Fig. 2F). CR augmented this phenotype, with 30mCR mice showing significantly longer time-to-peak tension and half-relaxation time than either 10mCON or 30mCON in both SOL and EDL muscles (Fig. 2F).

Consistent with the CR-induced fast-to-slow shift in muscle function properties, preferential protection of slow-twitch muscle mass, and improvements in whole-body endurance, fiber type-specific analysis of muscle cross sections showed a strong increase in the proportion of total cross-sectional area made up by slower fiber types in SOL, EDL, TA and TRI (Fig. 1G, H). Although a fast-to-slow transition was seen in all muscles analyzed, each muscle displayed specific changes in fiber type size and number (Supplementary Fig. 2A–E). Compared to 10mCON and 30mCON, the proportional area of type I fibers in SOL, IIX fibers in EDL, IIA fibers in TA and both IIA and IIX fibers in TRI was higher while the proportional area of IIX in SOL and IIB in EDL, TA and TRI was lower for 30mCR (Fig. 1G, H). The largest and fastest type IIB fibers appeared to be the most expendable for calorie restricted mice, with significant reductions in both proportional fiber number (Supplementary Fig. 2B) and minimum fiber feret (Supplementary Fig. 2C, D) in EDL, TA and TRI muscles. On the other hand, the size of slower IIA fibers and of intermediate IIX fibers were less affected by both age and CR (Supplementary Fig. 2C, D) and CR increased their proportional number (Supplementary Fig. 2B). Since slower-type fibers are more resistant to age-related atrophy, the CR-induced fast-to-slow fiber-type transition, despite the absolute decrease in muscle mass, may ultimately preserve muscle function in aging mice as seen with other interventions³¹.

Calorie restriction and rapamycin induce distinct transcriptomic changes. While the overt aging phenotype in calorie-restricted mice is distinct from that observed in mice treated with rapamycin over the same period¹³, calorie restriction is thought



to counteract aging in large part by suppressing nutrient-induced activation of mTORC1 activity³². If this were the case, then long-term CR and RM should induce a common core gene expression signature in aging muscle. To address this hypothesis, we performed mRNA-sequencing on four muscles (GAS, TA, TRI and SOL) from six 30-month-old calorie restricted mice and

compared the profiles with our previously reported 10mCON, 30mCON and 30mRM data sets (Fig. 3A)¹³.

To determine the overlap in core gene expression signatures induced by age, CR and RM, we first defined the specific effect of each condition separately by performing principal component (PC) analysis on data from all four muscles for each of the

Fig. 2 CR promotes a fast-to-slow muscle fiber phenotype shift. **A** Muscle mass for *quadriceps* (QUAD), *gastrocnemius* (GAS), *tibialis anterior* (TA), *plantaris* (PLA), *extensor digitorum longus* (EDL), *soleus* (SOL), and *triceps brachii* (TRI) was averaged across both limbs, normalized to body mass and then to 10-month-old control mice. **B** Scatterplots and linear regressions of the relationship between body and muscle mass of the fast twitch TA, TRI, GAS, QUAD and EDL muscles and the slow twitch SOL muscle. Isolated muscle function parameters, including **C** force-frequency curve (left) and fatigue response to multiple stimulations (right), **D** peak force normalized to body mass, **E** peak force normalized to cross sectional area (specific force), and **F** mean twitch responses including time-to-peak tension (TPT), half-relaxation time (1/2-RT) and peak twitch (Pt) for SOL (top panel) and EDL muscle (bottom panel). **G** Proportional total fiber-type-specific cross-sectional area analyzed on whole cross-sections of (left to right) SOL ($n = 6$), EDL ($n = 7, 9$ and 8), TA ($n = 11, 13$ and 7) and TRI ($n = 5, 9$ and 9) for 10mCON, 30mCON and 30mCR, stained with antibodies against type I (blue), type IIA (yellow), and type IIB (green) fibers as well as laminin (red), while fibers without staining were classified as IIX. **H** Representative magnifications of images from whole-muscle cross sections for SOL, EDL, TA and TRI, quantified in 2G and Supplementary Fig. 2. Group numbers for 10mCON are $n = 17$ (**A, B**), 10 (**C-F**: EDL) and 8 for fatigue, 11 (**C-E**: SOL) or 9 for fatigue, for 30mCON $n = 20$ (**A, B**), 19 (**C-F**: EDL), 15 (**C, D, F**: SOL) and 14 (**E**: SOL), and for 30mCR $n = 20$ (**A, B**), 18 (**C-E**: EDL) or 16 for fatigue, 15 (**C-E**: SOL) or 13 for fatigue, 12 (**F**: SOL) and 15 (**F**: EDL). Data are presented as mean \pm SEM. One-way (**A** and **D-F**) or two-way repeated-measure (**C, G**) ANOVAs with Fisher's LSD or Tukey's post hoc tests, respectively, were used to compare between data. *, **, and *** denote a significant difference between groups of $P < 0.05$, $P < 0.01$, and $P < 0.001$, respectively. Colored asterisks refer to the group of comparison.

following four comparisons: 10mCON vs. 30mCON ($PC_{10m-30m}$); 30mCON vs. 30mCR (PC_{30m-CR}); 30mCON vs. 30mRM (PC_{30m-RM}) and; 30mCR vs. 30mRM (PC_{CR-RM}). Aside from three prominent PC patterns representing the inter-muscle gene expression differences we have previously reported¹³, we found that for each comparison there was one PC (PC3 or PC4) that showed a clear between-group expression pattern difference common to all four muscles (Fig. 3B). To check to what extent genes aligned with $PC_{3_{10m-30m}}$ (aging effect), $PC_{4_{30m-CR}}$ (CR effect) and $PC_{4_{30m-RM}}$ (RM effect) overlapped, we created Venn diagrams for aging and CR, aging and RM and CR and RM effect comparisons, respectively (Fig. 3C). Strikingly, RM reversed and CR accentuated the vast majority of commonly regulated, age-related gene expression changes. Likewise, genes that responded to both CR and RM treatments were predominately regulated in the opposite direction. Gene ontology analysis showed that genes involved in extracellular matrix remodeling were highly represented in overlapping genes from each of the three comparisons (Fig. 3D).

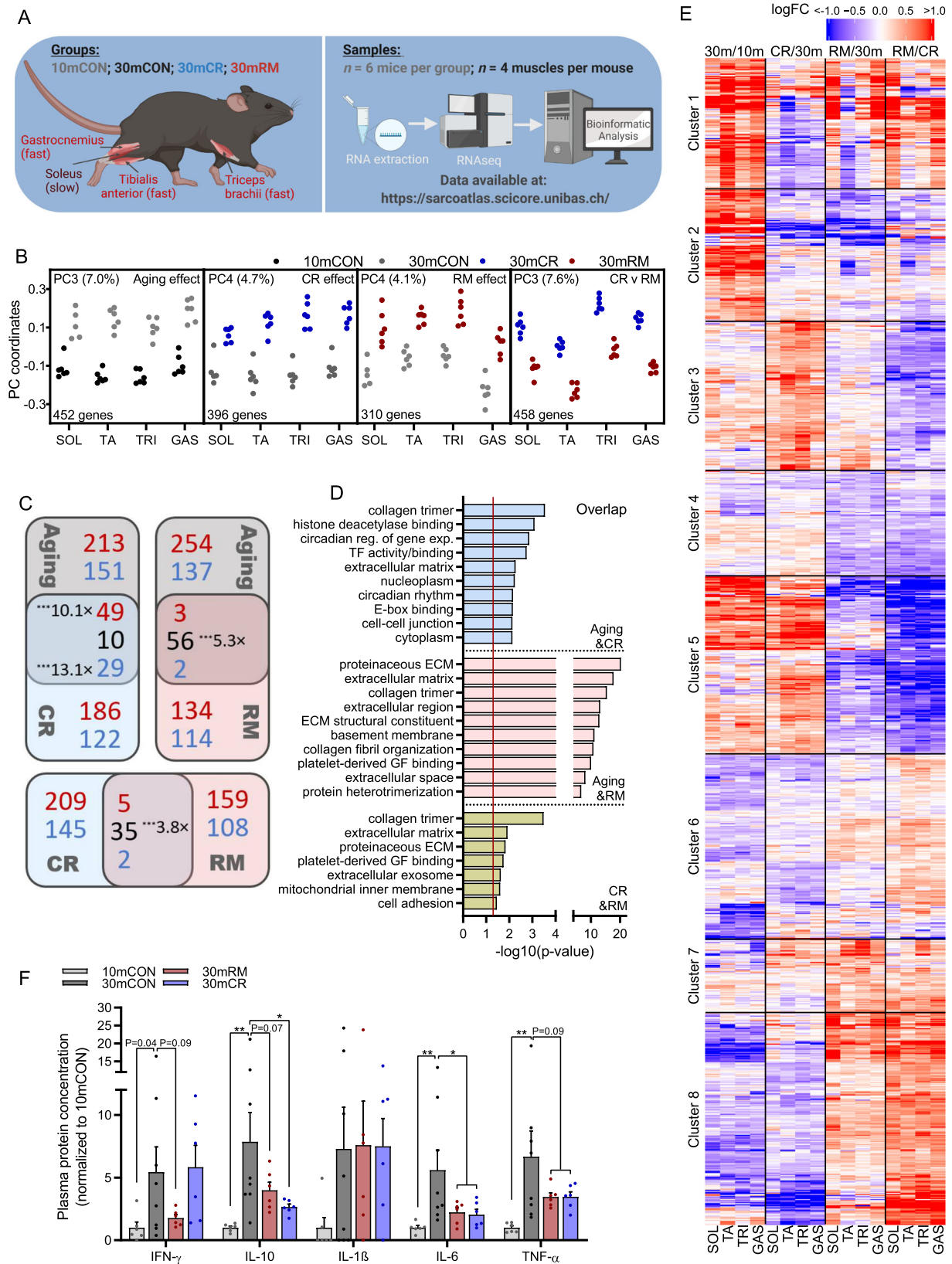
Next we visualized the log-fold changes in expression for each gene aligned to any of the PCs displayed in Fig. 3B. Hierarchical clustering based on the Euclidean distance of these changes rendered 8 gene clusters with distinct gene expression patterns (Fig. 3E). While CR and RM both tended to suppress a group of genes related to the innate immune response which are upregulated with age in cluster 2, CR and RM displayed strikingly opposing gene expression patterns throughout most other clusters as well as distinct CR (cluster 3) and RM (cluster 4) effects related to lipid metabolism and insulin signaling, respectively. While RM reversed, or partially reversed, age-related gene expression changes in many clusters, CR augmented age-related signaling such that gene expression differences between CR and RM were exaggerated. This pattern was particularly prevalent in cluster 5 and 8. Cluster 5 represents genes increased with age, further increased by CR and suppressed by RM, while cluster 8 displays the opposite pattern. The top DAVID gene ontology terms associated with cluster 5 relate to changes in metabolism while those associated with cluster 8 relate to the extracellular matrix (Supplementary Fig. 3). The common effects of CR and RM observed in cluster 2 primarily relate to immune responses. In line with these findings, circulating levels of the pro-inflammatory cytokines tended to be lower in both calorie-restricted and rapamycin-treated mice, with the exception of IFN- γ which tended to be suppressed by RM, but not CR (Fig. 1F).

These striking differences in gene expression patterns led us to wonder whether the signaling responses to CR and RM represent distinct paths to a common destination centered around immune and inflammatory suppression, i.e., an “all roads lead to Rome”

scenario, or whether CR and RM act on distinct muscle aging processes. If the latter is true, we reasoned that calorie restriction should benefit aging skeletal muscle independent of skeletal muscle mTORC1 suppression.

Calorie restriction attenuates muscle mTORC1-driven premature sarcopenia without suppressing mTORC1. To address this hypothesis, we calorie restricted male and female muscle-specific TSC1-knockout (TSCmKO) mice, which display sustained, nutrient-insensitive mTORC1 activation³³ and an accelerated aging phenotype^{13,26}. At 3 months of age, TSCmKO mice display high muscle mTORC1 activity and impaired autophagy, but mild phenotypic features. From ~6 to 12 months of age, TSCmKO display a progressive sarcopenia-like phenotype including muscle atrophy and weakness as well as accumulation of p62-labelled proteins and aggregates³³, which are also, to some degree, features of sarcopenia^{13,34}. We therefore tested whether 7 months of calorie restriction starting at 3 months of age can ameliorate the muscle fiber mTORC1-driven sarcopenic phenotype in TSCmKO mice (Fig. 4A). CR induced similar changes in body (Fig. 4B), fat (Fig. 4C) and lean (Fig. 4D) mass in both TSCmKO and WT control mice and comparable with those observed in naturally aging mice (Fig. 1B, D). Ad libitum-fed TSCmKO mice (TSC-AL) were significantly lighter than their ad libitum-fed controls (WT-AL) at 9.5 months. This was primarily due to a divergence in fat depositions from 4.5 months, with WT-AL gaining (+18%; $P < 0.05$) and TSC-AL losing (−25%; $P < 0.05$) fat mass over the period (Fig. 4B). Body mass and composition were comparable in calorie restricted TSCmKO (TSC-CR) and WT (WT-CR) mice, aside from a tendency for lower fat mass in TSC-CR than WT-CR at 6.5 months (Fig. 4B). CR also induced the characteristic metabolic adaptations in patterns of energy expenditure (Fig. 4E) and RER (Fig. 4F) equally in both WT and TSCmKO mice and comparable with those observed in naturally aging mice (Fig. 1K).

To confirm that mTORC1 activity was not suppressed in TSC-CR mice, we investigated the phosphorylation status of mTOR (S2448) and its key downstream targets S6 (S240/244 and S235/236) and 4EBP1 (S65) as well as Akt (S473) and PRAS40 (T246), which are dampened by inhibitory feedback from the mTORC1 target S6K1 via IRS1³⁵ in TA and/or GAS muscle using Western blot analysis (Fig. 4G, H and Supplementary Fig. 4A, B, D). TSC-AL mice displayed the stereotypical markers of chronic mTORC1 activation, including high phosphorylated mTOR, S6 and 4EBP1 as well as lower phosphorylated Akt and PRAS40. Despite reducing the availability of mTORC1-activating nutrients (e.g., amino acids), CR was largely incapable of suppressing mTORC1 activity or alleviating feedback inhibition of Akt in TSC-CR mice (Fig. 4G, H and Supplementary Fig. 4A, B, D). Together, these results indicate that CR induces typical changes in whole-body



composition and metabolism independent of muscle mTORC1 activity and without overt negative side-effects.

Despite a lack of effect on mTORC1 activity, CR robustly improved whole-body measures of muscular endurance (Hang test, Fig. 4I) and coordination (rotarod, Fig. 4J), independent of genotype. Likewise, CR improved or tended to improve both

specific force (Fig. 4K) and peak tetanic force normalized to body mass (Fig. 4L) in isolated SOL and EDL muscle in both WT and TSCmKO mice. Despite reducing absolute muscle mass in both WT and TSCmKO mice, CR reduced EDL (Supplementary Fig. 4E) and SOL (Supplementary Fig. 4F) absolute peak tetanic force only in WT mice, but not in TSCmKO mice

Fig. 3 CR and RM induce distinct gene expression signatures. **A** Scheme of treatment groups, muscles, and numbers of samples used in sequencing analysis. Data for 10mCON, 30mCON, and 30mRM have been previously reported¹³. **B** Coordinates of principal components representing aging (PC3 for 10mCON and 30mCON) CR (PC4 for 30mCON and 30mCR), RM (PC4 for 30mCON and 30mRM) and CR vs. RM (PC3 for 30mCR and 30mRM) effects for gene expression collected in *soleus* (SOL), *tibialis anterior* (TA), *triceps brachii* (TRI) and *gastrocnemius* (GAS). The fraction of variance in gene expression and the number of genes aligned (Pearson correlation coefficient ≥ 0.4 , z score projection ≥ 1.96) with each PC is displayed for each comparison. **C** Pairwise Venn diagram comparisons of genes significantly aligned to aging, CR and RM effects. Numbers in red, blue and black represent increasing, decreasing and oppositely regulated genes, respectively, with level of significance and representation factor denoted. **D** Top-ten DAVID gene ontology terms enriched ($P < 0.05$; gray and red dashed lines; one-sided, modified Fisher's exact test) for genes aligned to both aging and CR effects, aging and RM effects or CR and RM effects. **E** Heatmap of fold-changes for genes aligned with any of the four PCs described in **B** for all four muscles. Hierarchical clustering based on the Euclidean distance of these changes rendered 8 gene clusters. $n = 6$ mice per muscle per group, except for SOL 30mCON where one data point was removed due to a technical error. **F** Plasma cytokine protein concentration; $n = 6$ (10mCON), 8 (30mCON), 6 (30mCR) and 6 (30mRM). Data are mean \pm SEM and displayed as fold-change from 10mCON group. Cytokine levels below the fit curve range were set as 0. A one-way ANOVA with Fishers post hoc test was used to make comparisons between 10mCON and 30mCON, 30mCON and 30mRM and 30mCON and 30mCR. *, **, and *** denote a significant difference between groups of $P < 0.05$, $P < 0.01$, and $P < 0.001$, respectively. Where $0.05 < P < 0.10$, P values are reported. Experimental scheme in **A** created with BioRender.com.

(Supplementary Fig. 4G), suggesting improved muscle quality in TSC-CR mice. As we observed in aging WT mice, CR induced a slowing of muscle twitch properties, particularly in the SOL muscle (Fig. 4M, N), although fatigability was not significantly affected (Fig. 4O).

As a result of chronic mTORC1 activity-induced phosphorylation of ULK1 and thereby autophagy blockade, old (9–12 months) TSCmKO mice display strong cytosolic and aggregated p62 accumulation in muscle fibers and an associated increase in signs of muscle degeneration, including high levels of plasma CK and centro-nucleated, regenerating fibers³³. Indeed, TSC-AL mice displayed a strong increase in p62 aggregate- and cytosolic-positive fibers (Fig. 5A–C), p62 protein accumulation in muscle lysates (Fig. 5D), plasma CK activity (Fig. 5E) and centro-nucleated fibers (Fig. 5F). Strikingly, CR almost completely alleviated p62 accumulation and signs of muscle degeneration. Despite the strong reduction in p62 protein levels, CR did not suppress *Sqstm1* expression, which encodes for the p62 protein, nor the other autophagy induction mediators *Ctsl*, *Gabarrapl2*, *Bnip3*, *Atg7* or *Map1lc3a* (Fig. 5C). Likewise, the mTORC1-mediated phosphorylation of ULK1 (S757), the LC3II/LC3I ratio and protein levels of beclin1 and BNIP3 were all unaltered by CR (Fig. 5I–K). Furthermore, preliminary autophagic flux experiments showed that treatment of TSC and TSC-CR mice with the lysosome inhibitor, colchicine, failed to induce the strong LC3 II accumulation seen in WT-AL and WT-CR mice (Supplementary Fig. 5). These results indicate that the CR-induced reduction in p62 protein accumulation does not result from a CR-induced restoration of autophagic flux.

Endoplasmic reticulum (ER) stress and activation of the unfolded protein response (UPR) is also a hallmark of chronic muscle mTORC1 activation²⁶. CR did not reduce signs of ER stress in TSCmKO mice, including increased levels of ATF4, FGF21 and BiP (Supplementary Fig. 4C). However, CR altered the response to ER stress, blunting the mTORC1-driven upregulation of *Trib3* (Fig. 5L), which can bind and inhibit the breakdown of p62, while inducing *Xbp1* (Fig. 5M), encoding a UPR-inducing transcription factor³⁶. CR also induced the expression of *Keap1* (Fig. 5N), a gatekeeper protein for the NRF2-induced stress response that can be sequestered by p62, thereby preventing it from binding and preventing NRF2 nuclear translocation. While initially cytoprotective, chronic NRF2-induced activation of the stress response is deleterious³⁷. In line with a CR-induced suppression of NRF2 activity by *Keap1* upregulation, the mTORC1-induced upregulation of *Gsta1* expression, an NRF2 target, was strongly suppressed in TSC-CR mice (Fig. 5O).

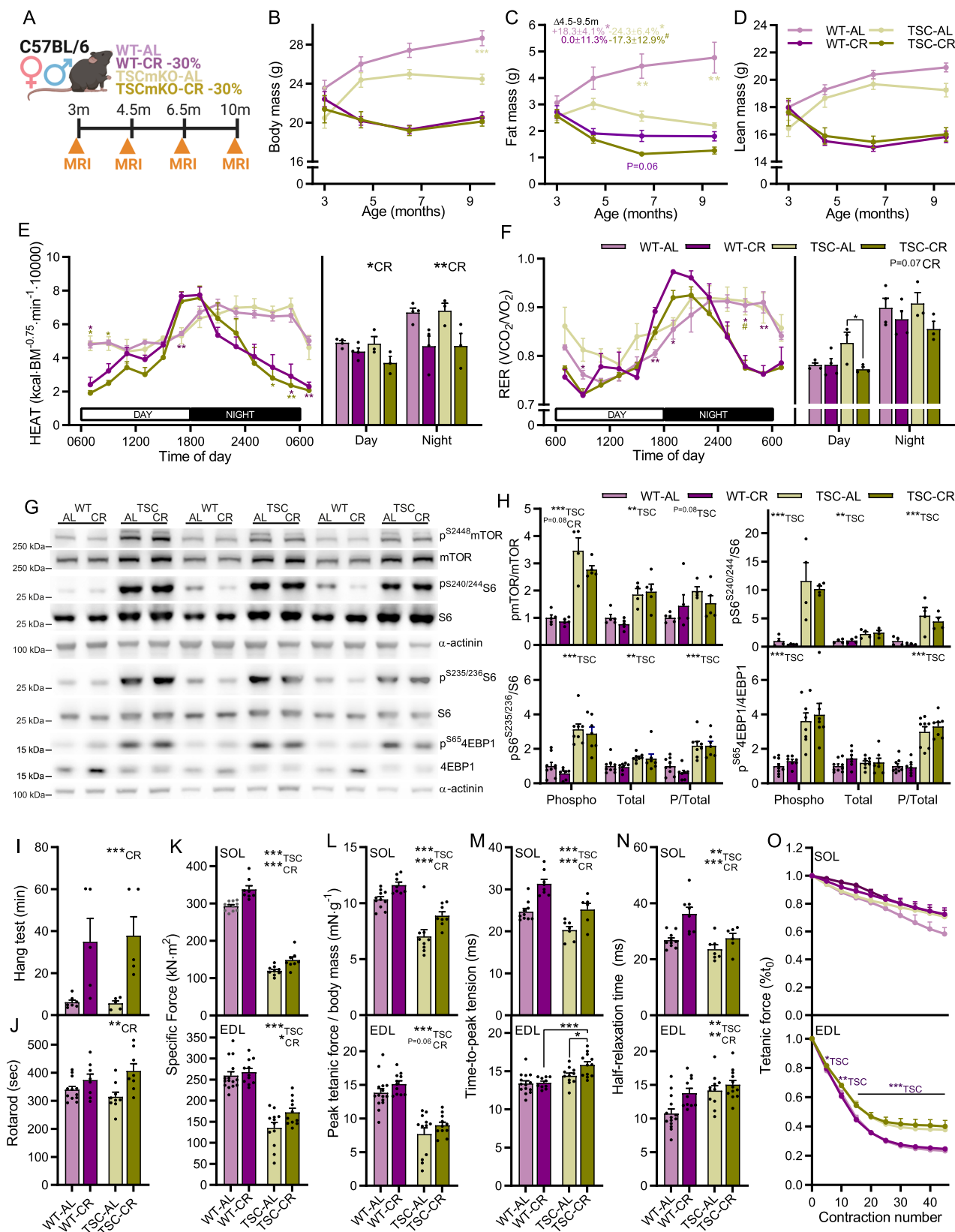
Together, these data strongly support the idea that CR can improve muscle proteostasis, integrity and function without

suppressing mTORC1 activity. But is the reciprocal also true, or are the beneficial effects of rapamycin-induced mTORC1 suppression on aging skeletal muscle already captured by CR? In other words, would rapamycin also slow muscle aging in CR mice?

CR and RM have distinct and often additive beneficial effects on aging skeletal muscle. To directly determine whether RM and CR exert non-overlapping effects in aging skeletal muscle, ad libitum-fed (CON) and 35% calorie restricted (CR) male C57BL/6 mice were fed a standardized AIN-93M diet containing either encapsulated rapamycin (RM and CR + RM) or an equivalent amount of encapsulating vehicle (Eudragit; CON and CR) starting from 19 months of age (Fig. 6A). Based on body mass and food intake data from our initial study and a target dose of $\sim 4 \text{ mg}\cdot\text{kg}^{-1}\cdot\text{day}^{-1}$ rapamycin, 42 and $48 \text{ mg}\cdot\text{kg}^{-1}$ of active encapsulated rapamycin was incorporated into the diet of RM and CR + RM groups, respectively. Consistent with our previous results, body mass loss compared to pre-trial levels was observed from 25 months in CON mice and from 20 months in RM-treated mice. After the initial adjustment to reduced food intake by 20 months of age, CR and CR + RM mice also displayed an age-related decline in body mass from around 26 months (Fig. 6B). Food intake, normalized to body surface area, was relatively stable over the treatment period in CON and RM mice, while CR and CR + RM mice showed a steady increase in normalized food intake from 20 months of age following an initial steep decline (Fig. 6C). RM did not alter the CR or age-related decline in whole-body fat mass and despite reducing lean mass in ad libitum-fed mice, RM did not alter the CR-induced decline in whole-body lean mass (Fig. 6D).

Repeated grip strength measurements spanning the treatment period showed a clear RM-induced attenuation in the progressive loss of both absolute and body mass normalized grip strength (Fig. 6E) starting at 24 months of age. CR also induced a strong increase in body mass normalized grip strength between 19 and 22 months, independent of RM treatment. RM and CR also induced distinct changes in voluntary wheel running activity. While CR increased both day and night-time running distance independent of RM treatment, RM increased night-time running distance independent of CR (Fig. 6F, G). CR also potentially improved inverted grid-hang time independent of RM treatment (Fig. 6H).

RM and CR individually induced changes in whole-body metabolism consistent with our previous observations¹³ (Fig. 6I, J). RM induced a consistent increase in energy expenditure normalized to body surface area in control mice, but not in CR mice (Fig. 6I), consistent with both RM and CR reducing non-functional tissue mass (Supplementary Fig. 6B, C). In contrast, RM blunted both the



CR-induced increase in RER during the first half of the night and the CR-induced decrease in RER during day-time hours (Fig. 6). As such, RM significantly reduced and CR significantly increased the range in whole-body RER over the 24h recording period, which could indicate opposing effects of RM and CR on metabolic flexibility³⁸. Since prolonged RM treatment is known to inhibit

mTORC2 and thereby glucose uptake, we wondered whether alterations in blood glucose or feeding behavior may explain the effect of RM on whole-body fuel utilization. Blood glucose was not different between CON and RM or between CR and CR + RM groups at 8 am or at 6 pm after a 10 h fast (Fig. 6K). Likewise, RM did not alter the blood glucose response to the reintroduction of

Fig. 4 CR improves muscle function without suppressing mTORC1 activity in the TSCmKO model of accelerated muscle aging. **A** Experimental design schematic. **B** Body, **C** whole-body fat, and **D** lean mass for WT and TSCmKO mice fed ad libitum (WT-AL and TSC-AL) or 70% of ad libitum (WT-CR and TSC-CR) beginning at 3 months of age. **E** Whole-body metabolic analysis of energy expenditure normalized to body surface area and **F** respiratory exchange ratio (VCO₂/VO₂; lower) reported every 2 h across one full day (white)/night (black) cycle (left) and day and night-time averages (right) in the month prior to endpoint measures; $n = 12$ (10mCON), 9 (30mCON), and 10 (30mCR) mice. **G** Representative western blot analysis of mTORC1 pathway components in *gastrocnemius* (GAS) muscle. **H** Quantification of western blots showing the abundance of phosphorylated protein normalized to total protein for mTOR, S6 and 4EBP1. **I** Inverted grid hang time and **J** time spent on a rotating rod. Isolated muscle function parameters for SOL (upper panel) and EDL (lower panel), including **K** specific force, **L** peak tetanic force normalized to body mass, **M** twitch time-to-peak tension, and **N** half-relaxation time as well as **O** fatigue response to multiple stimulations. For B-D, $n = 12, 8, 9$ and 8 except for the final time point where $n = 16, 13, 12,$ and 12 for WT-AL, WT-CR, TSC-AL and TSC-CR, respectively. For **E, F**, $n = 4, 4, 3,$ and 3 ; for G-H, $n = 9, 7, 8,$ and 7 (pS6^{S235/236} and p4EBP1^{S65}), $5, 5, 4,$ and 5 (pmTOR^{S2448}) and $4, 4, 4,$ and 4 (pS6^{S240/244}); for **I**, $n = 12, 8, 9$ and 8 ; for **J**, $n = 7, 5, 5$ and 5 ; for **K, L**, $n = 15, 11, 12, 11$ (EDL) and $11, 8, 9, 8$ (SOL); for **M, N**, $n = 14, 10, 11, 12$ (EDL) and $10, 8, 7, 6$ (SOL) and; for **O**, $n = 12, 9, 8, 8$ (EDL) and $8, 7, 6, 7$ (SOL) for WT-AL, WT-CR, TSC-AL and TSC-CR, respectively. Data are mean \pm SEM. Two-way ANOVAs with Tukey post hoc tests were used to compare the data. *, **, and *** denote a significant difference between groups of $P < 0.05$, $P < 0.01$, and $P < 0.001$, respectively. #Denotes a trend where $0.05 < P < 0.10$. Colored asterisks refer to the group of comparison. Experimental scheme in **A** created with BioRender.com.

food between 6 pm and 12 pm (Fig. 6K). CR mice ate their 2.1 g food allocation at a higher rate than ad libitum-fed mice (Fig. 6L). Interestingly, CR + RM mice ate their food allocation more slowly than CR mice, which may serve as a strategy to prevent high blood glucose levels in the face of a RM-induced impairment in glucose uptake.

Next we used two-way ANOVAs to determine whether CR and RM also exerted distinct, independent effects on muscle mass. Consistent with improvements in whole-body muscle function, significant CR main effects were observed for relative TA, QUAD, EDL, PLA, GAS, brachioradialis (BR) and biceps brachii (BIC) muscle mass (Fig. 7A). Again, the effects of RM were either distinct or additive to those of CR, with significant RM main effects for TA, QUAD, EDL, PLA, BR, BIC and TRI. As we have previously observed, specific muscles have different responses to specific interventions¹³. RM increased both relative and absolute muscle mass in the TRI muscle, while CR did not affect relative mass and reduced absolute TRI muscle mass (Fig. 7A and Supplementary Fig. 6A). On the other hand, CR, but not RM improved relative GAS muscle mass, while CR significantly reduced and RM tended to reduce absolute GAS mass. The only interaction effect for RM and CR was observed for the SOL muscle, where RM improved relative muscle mass in CR mice but not ad libitum-fed mice.

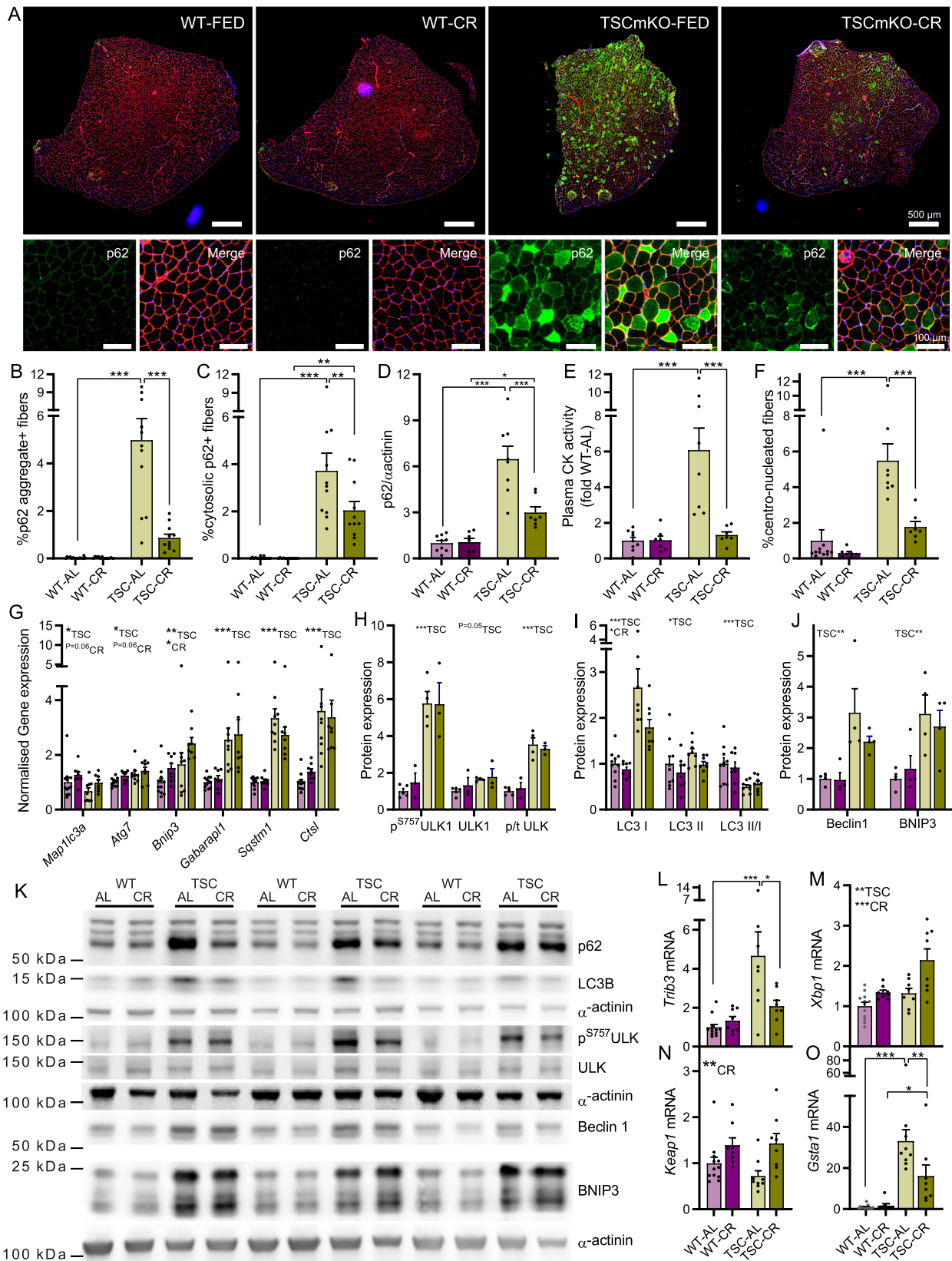
In line with the beneficial effects of RM treatment on whole-body muscle function and muscle size, independent of ad libitum or restricted feeding, RM main effects for in vitro muscle function properties were observed in the slow-twitch SOL muscle and to a lesser extent the fast-twitch EDL muscle (Fig. 7B–F). CR resulted in significant reductions in absolute tetanic force at multiple stimulation frequencies in the SOL (Fig. 7B, upper) and EDL (Fig. 7B, lower). RM significantly increased absolute tetanic force from a stimulation frequency of 20 Hz in SOL, but not EDL muscle. Despite initial contraction forces below that of ad libitum-fed mice, tetanic force in calorie restricted mice approached that of ad libitum-fed mice after 20 contractions in SOL (Fig. 7C, upper) and from 30–35 contractions in EDL (Fig. 7C, lower). RM, but not CR, induced significant increases in peak tetanic force normalized to body mass in both SOL (Fig. 7D, upper) and EDL (Fig. 7D, lower). Rapamycin also induced a significant increase in muscle quality, as evidenced by higher specific forces in SOL muscle (Fig. 7E, upper) independent of feeding status and in EDL muscle (Fig. 7E, lower) from ad libitum-fed mice. Analysis of muscle twitch properties show that RM tends to slow SOL time-to-peak tension (TPT), while CR slowed EDL TPT (Fig. 7F). CR slowed and RM tended to slow half-relaxation times in SOL muscle, while CR induced a slowing of half-relaxation time in EDL.

Finally, we have shown that CR promotes a fast-to-slow fiber type transition (Fig. 2G, H) while RM also promotes a fast-to-slow fiber type transition and additionally increases the size of IIA and IIX fibers¹³. Based on the preferential effect of both CR and RM on slow-twitch fibers and our previous observations that RM exerts negative side effects in some hindlimb muscles that may relate to their susceptibility to denervation, we analyzed the fiber-type composition and fiber cross sectional area in BR muscle, a forelimb muscle involved in grasping and arm flexion that contains a high proportion of IIA and IIX fibers (Fig. 7G–J). In BR muscle, both CR and RM independently increased the size of IIA and IIX fibers, with main effects for both treatments (Fig. 7H). Likewise, both CR and RM showed main effects for higher IIA fiber number and lower IIB fiber number (Fig. 7I), an effect also induced by age alone. Together, the increase in IIA fiber size and number and the parallel decrease in IIB fiber number observed with age, CR and RM resulted in a change in proportional total fiber area from 13.6, 37.3 and 49.1% for IIA, IIX and IIB fibers in 10-month-old adult mice to 38.1, 46.6 and 15.3% for IIA, IIX and IIB fibers in CR + RM treated mice (Fig. 7J). A comparable, although less pronounced additive effect of CR and RM on the fast-to-slow fiber type shift was also seen in the slow-type SOL muscle (Supplementary Fig. 7). However, in contrast to BR muscle, IIA fiber size was not altered in the SOL muscle from CR + RM mice compared to CON or CR mice.

Together, these data confirm that both CR and RM treatment exert distinct and often additive effects on whole-body muscle function and metabolism, the size and fiber type composition of specific muscles as well as isolated muscle function properties and molecular signatures (Fig. 8). Therefore, these findings support the idea that long-term mTORC1 suppression via RM can benefit aging skeletal muscle independent of CR.

Discussion

The mechanism underlying the potent and robust anti-aging effects of CR have long fascinated the research community. An early theory proposed mTORC1 suppression as a central part of CR-induced longevity⁸. Research showing long-term RM treatment extended lifespan in mice seemed to confirm this theory⁷. However, despite both CR and RM blunting mTORC1 activity and promoting autophagy^{18,19}, their effects on insulin signaling and glucose tolerance diverge^{19,20} and molecular profiles following short-term CR and RM in adult mouse liver show predominately distinct signatures^{21,22}. Our multi-muscle transcriptomic data from 30-month-old mouse muscle support the concept that CR and RM have distinct mechanisms. Importantly, our study compares the effects of CR and RM treatment during the entire period of sarcopenic development (15 to 30 months), therefore representing both



signaling responses to CR and RM as well as the cumulative effect of the treatments on age-related signaling. To improve the current understanding of the molecular mechanisms contributing to sarcopenia, we made our data publicly available through the user-friendly web application SarcoAtlas (<https://sarcoatlas.scicore.unibas.ch/>), building on our previously released sarcopenia data sets^{13,14}.

The divergent gene expression patterns induced by CR and RM do not necessitate that entirely non-overlapping mechanisms are responsible for the beneficial effects of CR and RM. Rather, while starting from different points, these treatments could converge on the same effector pathways. Here we addressed the question of whether CR-induced mTORC1 suppression is sufficient to make

Fig. 5 CR attenuates p62 accumulation and improves muscle integrity in TSCmKO mice. **A** Representative *tibialis anterior* (TA) cross sections stained with antibodies against p62 and laminin and counterstained with DAPI. Quantification of fibers with **B** p62+ aggregates and **C** p62+ cytosolic staining. **D** Western blot quantification of p62 protein expression in gastrocnemius muscle. **E** Plasma creatine kinase activity and **F** percentage centro-nucleated fibers in WT-AL, WT-CR, TSC-AL and TSC-CR mice. **G** RT-qPCR analysis of autophagy associated genes in gastrocnemius muscle. Western blot quantification of the abundance of **H** phosphorylated and total ULK1 protein, **I** LC3I, LC3II and the ratio of LC3II to I, and **J** beclin1 and BNIP3 protein as well as **K** representative gels. Two and three independent blots were performed for p62 and LC3B, respectively. RT-qPCR analysis of ER-stress and autophagy interacting genes, including **L** *Trib3*, **M** *Xbp1*, **N** *Keap1*, and **O** *Gsta1*. For **B, C**, $n = 15, 12, 11, 11$; for **D, E**, $n = 9, 7, 8, 7$; for **F**, $n = 11, 7, 8, 7$; for **G** and **N, O** $n = 12, 8, 9, 8$; for **H**, $n = 5, 3, 4, 3$; for **I**, $n = 10, 8, 8, 8$; for **J**, $n = 4, 4, 4, 4$, for **L, M**, $n = 12, 8, 8, 8$ and; for **N, O**, $n = 12, 8, 9, 8$ for WT-AL, WT-CR, TSC-AL, and TSC-CR, respectively. Data are presented as mean \pm SEM. Two-way ANOVAs with Tukey post hoc tests were used to compare data. *, **, and *** denote a significant difference between groups of $P < 0.05$, $P < 0.01$, and $P < 0.001$, respectively. #Denotes a trend where $0.05 < P < 0.10$. Colored asterisks refer to the group of comparison.

RM redundant and vice versa, and provided definitive evidence that CR and RM exert non-overlapping and often complementary effects in aging mouse skeletal muscle. Specifically, CR improves skeletal muscle function and quality independent of mTORC1 suppression and RM improves skeletal muscle function in CR mice. While mTORC1 inhibition as a strategy to fight aging arose from attempts to pharmacologically reproduce CR, the implications stemming from the apparent invalidation of this assumption are far greater to the aging field. Assuming that a true CR mimetic can eventually be identified, the prospect of multiple, additive interventions to slow aging is an exciting prospect.

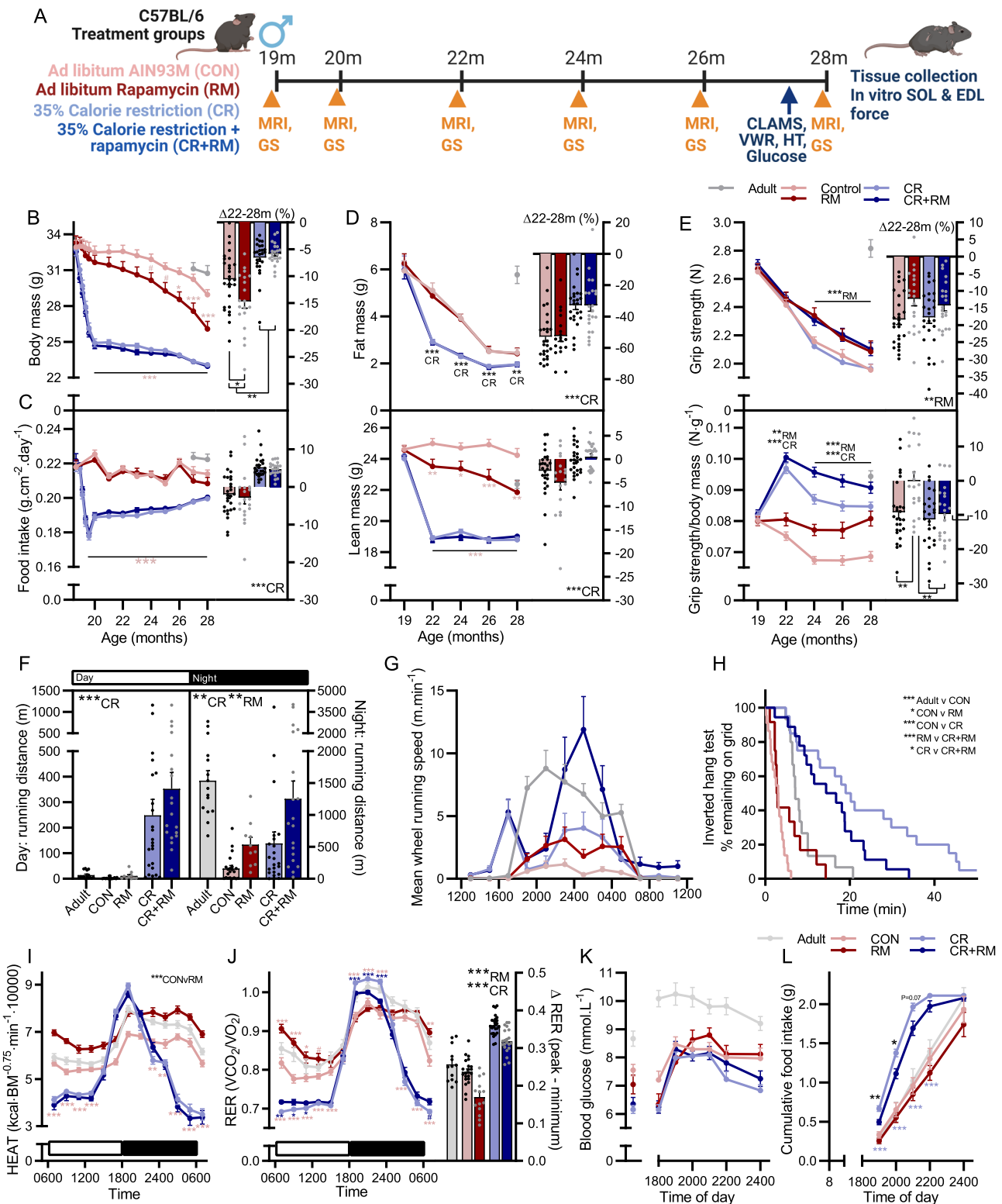
While the specific mechanisms responsible for the pro-longevity effects of CR have proved challenging to pin down, many plausible theories have been developed. The evolutionary model of CR proposes that under energy scarcity, an organism actively allocates energy towards somatic maintenance at the expense of reproduction, thereby extending lifespan in the hope that circumstances will sufficiently improve to once again support reproduction^{39,40}. This theory is supported by observations that CR promotes the expression of maintenance and repair processes^{41,42}. Signs of a CR-induced promotion of somatic maintenance was also observed in TSCmKO mice in the absence of mTORC1 suppression or reduced ER stress (Fig. 5). A CR-mediated induction of the somatic maintenance genes *Xbp1* and *Keap1* was associated with less p62 accumulation and improved skeletal muscle integrity (Fig. 5), highlighting the fact that skeletal muscle fiber mTORC1 suppression is not solely responsible for the beneficial effects of CR on muscle homeostasis.

The evolutionary model assumes that CR-induced physiological changes are inherently pro-longevity, however, long-term CR may impair regenerative potential in mice⁴³ and when returned to an energy-rich diet, calorie restricted *Drosophila melanogaster* reproduce less and experience greater mortality than their age-matched, non-restricted counterparts². Likewise, the beneficial effects of CR are quickly lost upon refeeding in rodents⁴⁴ and in humans, metabolic adaptations to CR promote strong weight gain upon refeeding⁴⁵. Therefore, rather than actively promoting longevity, CR may provide an escape from the cost of an energy-rich diet². The fact that sedentary, ad libitum-fed mice often become obese in aging studies¹² and that the propensity of mouse strains to become obese strongly correlates with the longevity effects of CR⁴⁶ support this theory. Importantly, in our study we used a combination of an AIN-93 maintenance diet and a controlled feeding regime to limit the food intake of ad libitum-fed mice with a penchant for overeating (Fig. 1), thereby limiting the potential negative effects of an obese and unhealthy control group, a common criticism of CR experiments⁴⁶.

An alternate theory proposes that rather than an evolved, programmed tradeoff between somatic maintenance and reproduction, the pro-longevity effects of CR may simply result from a passive, serendipitous response to metabolic stress² such as a

lower metabolic rate⁴⁷, reduced mTORC1 activity⁸ or hormetic response⁴⁸. In line with such an interpretation, long-term CR did not slow the absolute loss of all-limb grip strength nor did it reverse age-related gene expression changes. However, the CR-induced alterations in body composition led to marked improvements in body mass-normalized grip strength, which proceeded to decline with age in line with ad libitum-fed mice, but from a new higher starting point (Figs. 1 and 6). Irrespective of the permanence of CR-induced longevity and whether the effects are actively or passively conferred, the strong link between CR and beneficial health and lifespan outcomes means that closely examining the molecular and physiological responses to CR is a promising avenue to identify pathways and phenotypes that can be exploited to improve muscle function and consequently, the quality of life of aging individuals. The same is true for the pro-longevity and anti-sarcopenic effects of rapamycin. While our rationale for comparing these two interventions originally centered on identifying a core set of pathways regulated by aging and commonly counter-regulated by CR and RM, our data show that CR and RM induce strikingly distinct gene expression profiles, with those genes and pathways that do overlap being regulated in predominately opposing directions (Fig. 3).

For example, CR specifically increases genes involved in lipid metabolism and RM specifically suppresses genes involved in insulin signaling, while the strongest counter-regulated gene expression cluster maps to ECM remodeling, including many collagen genes, which are reduced in aging muscle, restored by rapamycin but further decreased by CR. ECM gene expression coincides with changes in muscle size, increases during muscle hypertrophy⁴⁹, and decreases during experimental muscle atrophy⁵⁰ as well as sarcopenia in rodents^{13,14,51,52}. Declining collagen expression has also been linked to organismal aging, while autophagy-inducing interventions restore collagen expression and promote longevity^{53,54}. While this opposing action of CR and RM on ECM gene expression could be seen as counteractive, it may also represent different means of addressing the same perturbation. That is, age-related stressors can be counteracted by either blunting the perturbation or enhancing the inherent coping mechanisms. Indeed, gene expression profiling studies show that changes in gene expression resulting from mutations in mice that shorten lifespan positively correlate with mutations and interventions that extend lifespan⁵⁵. In other words, organisms naturally boost stress responses to cope with life-shortening perturbations, while interventions that moderately stimulate these stress responses, such as CR, extend lifespan. Alternatively, changes in ECM gene expression may simply reflect changes in protein turnover or absolute muscle size induced by the treatment. In line with this hypothesis, CR blunts and RM boosts polysome loading, an indicator of protein turnover, in skeletal muscle²². The complexity of biological responses to aging and treatments such as CR and RM make interpreting



directionality of gene expression changes inherently challenging. It is therefore imperative that molecular profiles be accompanied by thorough phenotypic characterizations.

Perhaps the most strikingly consistent muscle phenotype displayed by CR mice was a fatigue resistant, fast-to-slow muscle fiber property switch, including an increase in number and proportional cross sectional area covered by slower-type fibers across five different muscles as well as slower twitch properties (Figs. 2 and 7) and

higher whole-body relative muscle endurance (Figs. 1 and 6). A similar, although less pronounced phenotype was also observed in response to long-term RM treatment¹³ (Fig. 7). Despite this seemingly overlapping effect of the two treatments, the CR- and RM-induced fast-to-slow fiber type conversion was additive in the forelimb *brachioradialis* muscle of CR + RM treated mice (Fig. 7). Since slower-type fibers are more resistant to age-related atrophy, the CR-induced fast-to-slow fiber-type transition, despite the

Fig. 6 RM and CR exert distinct and additive effects on whole-body muscle function and metabolism. **A** Experimental design schematic showing experimental groups as well as time course of physiological measures. Repeated measures (left) of **B** body mass, **C** food intake normalized to body surface area, **D** whole-body fat (upper), and lean (lower) mass as well as **E** absolute (upper) and body mass normalized (lower) all-limb grip strength measured across the treatment period from 19 to 28 months as well as the percentage change between 22 months after adaptation to CR and 28 months (right). **F** Day and night-time voluntary running distance and **G** running speed patterns across a 24 h period, as well as **H** Kaplan–Meier plot for the inverted grid-hang test performed prior to endpoint measures at 28 months. Whole-body metabolic analysis of **I** energy expenditure normalized to body surface area and **J** respiratory exchange ratio reported every 2 h across one full day (white)/night (black) cycle in the month prior to endpoint measures. **K** blood glucose levels and **L** voluntary food intake over the night-time feeding period following a day-time fast in 10mCON, 28mCON, 28mRM, 28mCR and 28mCR+RM groups. For **B–E**, $n = 15$ (Adult), 27 (CON), 19 (RM), 25 (CR), 22 (CR + RM). For **F, G**, $n = 15$ (Adult), 21 (CON), 10 (RM), 23 (CR), 19 (CR + RM). For **H**, $n = 15$ (Adult), 21 (CON), 12 (RM), 20 (CR), 18 (CR + RM). For **I, J**, $n = 13$ (Adult), 22 (CON), 14 (RM), 25 (CR), 21 (CR + RM). For **K, L**, $n = 15$ (Adult), 15 (CON), 12 (RM), 20 (CR), 18 (CR + RM). Data are presented as mean \pm SEM. Two-way ANOVAs with Tukey post hoc tests (**A–G** and **I–L**) and Mantel–Cox log rank tests (**H**) were used to compare the data. *, **, and *** denote a significant difference between groups of $P < 0.05$, $P < 0.01$, and $P < 0.001$, respectively. #Denotes a trend where $0.05 < P < 0.10$. Colored asterisks refer to the group of comparison. Experimental scheme in **A** created with BioRender.com.

absolute decrease in muscle mass, may ultimately preserve muscle fiber number and function in aging mice, as previously observed in muscle-specific BDNF knockout mice, which display a fast-to-slow fiber type transition and increased resistance to age-related muscle loss³¹.

A specific feature of CR believed to contribute to its beneficial effects in rodent skeletal muscle is an increase in physical activity prior to feeding¹⁷, and may at least partially explain the fast-to-slow fiber transition. This anticipatory behavior, reminiscent of exercise training, is not seen in ad libitum-fed mice and was not altered by RM in the current study (Fig. 6). As these studies were performed in sedentary mice, it is unclear to what extent the CR-induced quasi exercise stimulus would overlap with the known benefits of long term exercise, which has also been shown to induce pleiotropic effects that benefit aging muscle, including immune suppression, enhanced muscle oxidative capacity and a lean phenotype^{56,57}. Indeed, lifelong voluntary wheel running activity provides some additional benefits to aging muscle in rats undergoing mild (8%) CR⁵⁸, although this level of restriction may be insufficient to induce behavioral changes⁵⁹. Since muscle adaptations to exercise are accentuated by protein intake immediately before, during or after exercise, the close temporal restriction of activity and food intake in CR mice may be advantageous for maintaining muscle function with age. Although the CR-induced quasi exercise training is an artefact of experimental circumstance not applicable to humans, the combined impact of CR, including any benefits afforded through behavioral changes were on top of those induced by RM, particularly with regard to slowing of muscle fiber properties, relative grip strength and voluntary running distance (Figs. 6 and 7). While it will be important to determine whether RM impedes muscle adaptations to long-term exercise training in aging humans, as it does for muscle growth stimuli in young mice¹⁰, our data show that RM does not blunt muscle adaptations to CR and in fact accentuates many of them.

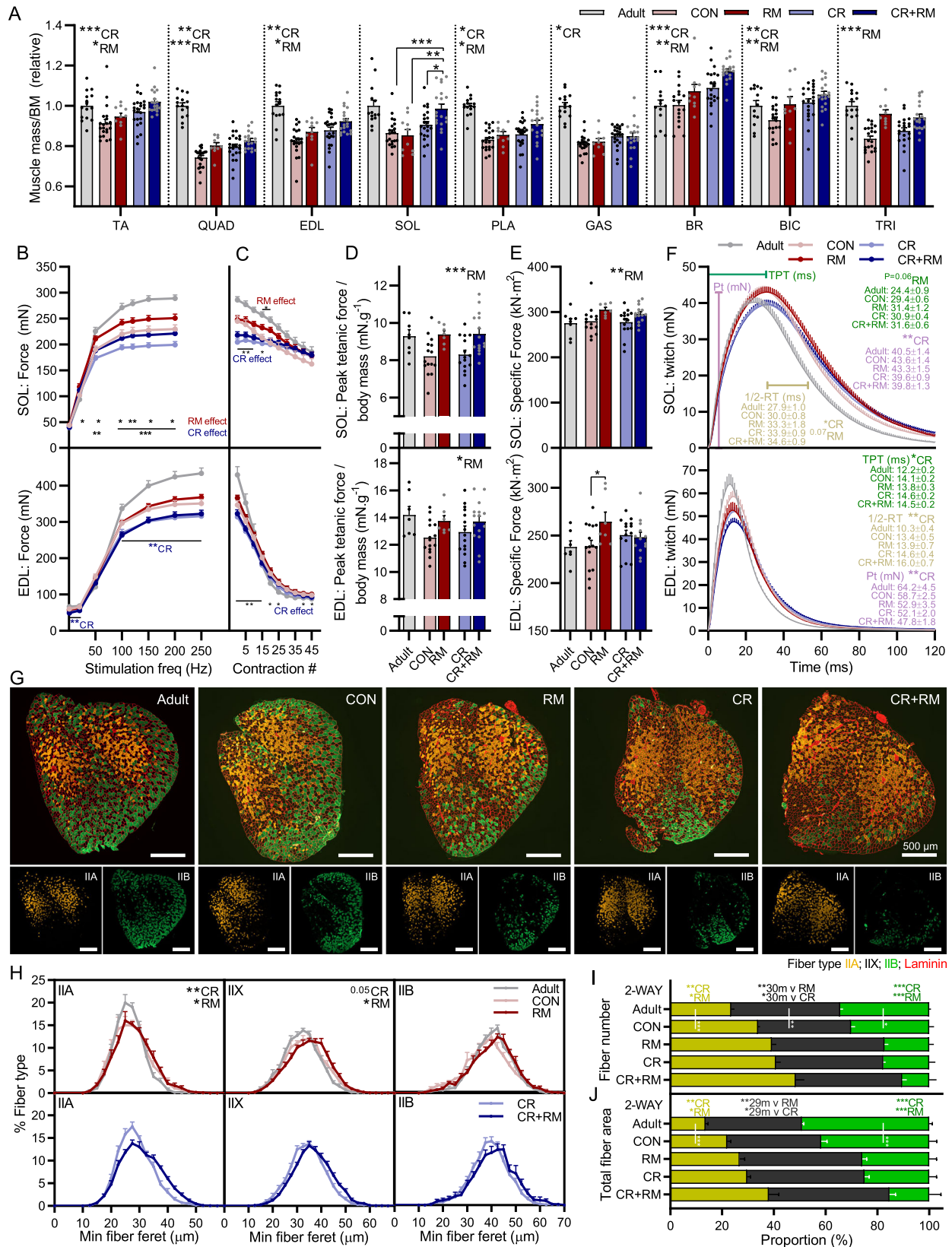
As sex differences have been noted in the specific physiological responses to aging, CR and RM and the optimal level of calorie restriction and rapamycin dose appears to differ, at least for lifespan extension^{43,60,61}, the specific responses to CR and RM observed in the current study may vary in naturally aging female mice. However, at optimal RM doses and calorie restriction levels, if anything, RM and CR have both been shown to be more effective at extending lifespan in female than male mice^{7,62}.

While together, our experiments clearly demonstrate that the beneficial effects of CR on muscle do not require mTORC1 suppression and likewise RM treatment is not redundant in restricted mice, the complementary mechanisms allowing the effects of these interventions to compound are less clear. Both CR and RM are well-known to reduce mTORC1

activity, but unlike in RM-treated mice, mTORC1 activity still responds to food intake in CR mice, although its activity is more temporally restricted, and decreases more during fasting periods than in ad libitum-fed mice⁶³. Since transient mTORC1 activity remains important in specific tissues, most blatantly highlighted by the severe testicular degeneration experienced by RM-treated mice, but also under growth conditions in skeletal muscle¹⁰, it might be expected that CR would represent a more favorable intervention to counter the detrimentally hyperactive mTORC1 frequently observed in aging tissue. Strikingly, our data point in the opposite direction, at least in sedentary mice, suggesting that CR-induced mTORC1 suppression is not sufficient to confer all the beneficial effects of RM treatment. Of course, whether this effect relates directly to muscle tissue mTORC1 suppression or via secondary effects of non-muscle tissue mTORC1 suppression is unclear.

Another explanation for the additive effects of CR and RM, could be co-compensation of treatment-specific side effects. A prime example relates to glucose tolerance, which is markedly improved in CR mice (Fig. 1), and impaired by RM⁶⁴. However, blood glucose levels were not habitually high in RM or CR + RM groups, instead, CR + RM-treated mice appeared to curb the ravenous consumption of daily food allocation seen in CR mice, thereby distributing energy availability over a prolonged period (Fig. 6K, L). Metabolic analyses showed that this subdued rate of food intake coincided with a lower RER during the early night-time eating phase but also a higher RER during the early day-time inactive period in CR + RM compared to CR mice (Fig. 6J). This could also be viewed as divergent impacts of CR and RM on metabolic flexibility³⁸, a concept referring to the ability of an organism to respond to changes in metabolic demand, with RM reducing and CR enhancing the magnitude of the switch in fuel utilization between day and night hours. Whether CR-induced increases in metabolic flexibility counteract RM-induced impairments remains to be tested. Along a similar line, we previously reported that specific muscles respond differently to rapamycin, an effect correlated with the presence (muscle not protected by RM, i.e., GAS) or absence (muscle protected by RM, i.e., TRI and TA) of pro-sarcopenic side effects¹³. Although a CR-induced amelioration of these negative effects of RM could explain the combined effects, the same muscle-specific effects of RM were observed in CR + RM mice, with less age-related muscle loss in the TRI and TA, but not in the GAS (Fig. 7A), hinting that further attenuation in muscle aging may be possible beyond combined CR and RM.

Together, our results conclusively demonstrate that CR and RM exert distinct, non-overlapping and frequently additive effects in aging skeletal muscle. The striking failure of RM to recapitulate the effects of CR and more surprisingly, the failure



of CR to recapitulate the effects of RM raises the exciting prospect of multiple, additive interventions to counteract sarcopenia. Further work is needed to systematically isolate targetable processes and examine the resulting interactions in order to develop optimal strategies to counteract sarcopenia and promote healthy aging.

Methods

Animal care. All procedures were performed in accordance with Swiss regulations for animal experimentation and approved by the veterinary commission of the Canton Basel-Stadt. Male, C57BL/6J mice for aging studies were purchased from the aging colony at Janvier Labs (Le Genest-Saint-Isle, France). Transgenic TSCmKO mice and their genotyping were previously described^{33,65}. Female and male TSCmKO and control littermates, floxed for *Tsc1* but not expressing

Fig. 7 CR and RM have additive effects on muscle mass, function and fiber size and composition. **A** Muscle mass for *tibialis anterior* (TA), *quadriceps* (QUAD), *extensor digitorum longus* (EDL), *soleus* (SOL), *plantaris* (PLA), *gastrocnemius* (GAS), *brachioradialis* (BR), *biceps brachii* (BIC) and *triceps brachii* (TRI) were averaged across both limbs, normalized to body mass and then to 10-month-old control mice. Isolated muscle function parameters, including **B** force–frequency curve and **C** fatigue response to multiple stimulations, **D** peak force normalized to body mass, **E** peak force normalized to cross sectional area (specific force), and **F** mean twitch responses including time-to-peak tension (TPT), half-relaxation time (1/2-RT) and peak twitch (Pt) for SOL (top panel) and EDL muscle (bottom panel). **G** Representative cross sectional images along with **H** fiber-type-specific minimum fiber feret distribution showing ad libitum-fed (upper) and calorie restricted (lower) groups, **I** fiber type-specific fiber numbers, and **J** total fiber-type-specific cross-sectional area of the forelimb BR muscle stained with antibodies against type I (blue), type IIA (yellow), and type IIB (green) fibers as well as laminin (red), while fibers without staining were classified as IIX. For **A**, group numbers are $n = 15$ (14 for SOL, 13 for BR and BIC; Adult), 21 (17 for BR, 19 for BIC; CON), 10 (9 for TRI; RM), 23 (22 for SOL and BIC, 21 for BR and TRI; CR) and 19 (18 for BR and BIC; CR + RM). For **B**, **D–F** (SOL), $n = 8$ (Adult), 15 (CON), 7 (RM), 15 (CR) and 15 (CR + RM). For **C** (SOL), $n = 8$ (Adult), 15 (CON), 7 (RM), 12 (CR) and 14 (CR + RM). For **B**, **D–F** (EDL), $n = 7$ (Adult), 15 (CON), 7 (RM), 14 (CR), 15 (CR + RM). For **C** (EDL), $n = 4$ (Adult), 14 (CON), 7 (RM), 12 (CR) and 14 (CR + RM). For **G**, **H**, $n = 6$ (Adult), 5 (CON), 6 (RM), 8 (CR) and 8 (CR + RM). Data are mean \pm SEM. Two-way repeated-measure ANOVAs with Tukey's post hoc tests were used to compare between data. *, **, and *** denote a significant difference between groups of $P < 0.05$, $P < 0.01$, and $P < 0.001$, respectively. Colored asterisks refer to the group of comparison.

HSA-Cre-recombinase, were used. For all studies, mice were kept in single cages under a fixed 12 h light–dark cycle (6 a.m. to 6 p.m.) at 22 °C (range 20–24 °C) and 55% (range 45–65%) relative humidity and were acclimatized to individual housing and the control diet for 3–4 weeks before the start of the experiment.

Aging studies. In the first aging study (results presented in Figs. 1–3), two independent groups of male mice were calorie restricted starting at 20 ($n = 11$) or 15 ($n = 21$) months of age. 10mCON, 30mCON and 30mRM data were generated alongside 30mCR, but data from these groups have largely been previously reported¹³. For appropriate interpretation of the previously unreported CR data, 10mCON and 30mCON data have been included. For combined CR + RM experiments (Figs. 6 and 7), all groups and data were newly generated. After 1-month acclimatization to individual housing and the standardized AIN-93M diet (TestDiet, 58M1-9GH6) containing 488 ppm Eudragit (Emtora), food intake of 19-month-old CR mice was incrementally reduced to 90, 80, and 70% for 1 week each before being maintained at 65% of mean baseline food intake. To avoid malnutrition, the concentration of vitamins and minerals were increased 1.43 \times in CR mice (58M1-9GH8). Rapamycin treated ad libitum-fed and CR mice received an AIN-93M diet containing 42 or 48 mg·kg⁻¹ active encapsulated (Eudragit) rapamycin (TestDiet, 58M1-9GH7), respectively. The concentration of RM was increased in CR + RM mice in an attempt to counter the discrepancy between body weight (~22%) and food intake reductions (~35%) and deliver a similar dose of rapamycin per kg body weight. In the week before starting the experiment, food intake, body mass and composition (via EchoMRI) and grip strength were measured and used to balance group selection. Each group (CON, CR, RM and CR + RM) contained mice with an almost identical mean and standard deviation for each measurement within experimental groups. Food intake and body mass were measured weekly. As previously described¹³, weight gain and obesity was limited in ad libitum-fed mice via daily food restriction to that of the control group mean (3.1 g) in mice with a propensity for overeating and weight gain.

TSCmKO studies. Mice were progressively adapted to calorie restriction by incremental reductions in food intake of 10% per week starting at 12 weeks of age, with mice receiving 70% of the genotype mean at the start of the third week. Baseline food intake was determined over a 3-week period prior to CR. Ad libitum-fed WT and TSCmKO mice ate 3.05 and 3.45 g day⁻¹ food, respectively, under baseline conditions. After CR habituation, WT-CR and TSC-CR groups were therefore given 2.1 and 2.4 g day⁻¹ food for 6 months. These experiments were performed over three separate trials using both female and male mice and either an AIN-93M standardized diet (D10012M; KLIBA NAFAG) or a standard chow diet (KLIBA NAFAG-3432). Since results were comparable across all trials, food and sexes, data were pooled for analysis.

Body composition analysis. Fat mass and lean mass were measured on restrained, conscious mice using an EchoMRI-100 (EchoMRI Medical Systems).

Whole-body muscle function. Mice were initially familiarized to voluntary running wheels over a 48–72 h period. Mice were then given free access to voluntary running wheels for a 24 h period every two months in the first study and once for a 48 h period in the subsequent CR + RM study, with data for the final 24 h used for analysis. Inverted grid hang time was measured by placing mice on a wire grid, which was slowly turned upside down and positioned over a ~40 cm high box containing a foam pad at the bottom. Performance was taken as the longest time a mouse could hold onto the grip across three trials separated by at least 30 min. All-limb grip strength was measured using a small grid attached to a force meter (Columbus Instruments). Mice firmly holding the grid with all four paws were gently pulled horizontally at a consistent speed until the grasp was broken. Performance was taken as the median of 3–5 trials with at least 10 min rest between

tests. Trials in which the mouse actively pulled on the grid while the test was underway were discarded. The same researcher performed all grip strength measurements at a similar time of day.

Comprehensive laboratory animal monitoring system (CLAMS). CLAMS (Columbus Instruments, Columbus, OH) was used to measure whole-body metabolic parameters including energy expenditure, oxygen consumption (VO₂), CO₂ production (VCO₂) and the ratio of VCO₂ to VO₂ or respiratory exchange ratio (RER), as well as locomotor activity. RER is dependent on energy substrate utilization, ranging from above 1 to 0.7, which indicates preferential use of carbohydrates and lipids, respectively. Locomotor activity was measured on X, Y and Z axes using infrared beams. Energy expenditure was calculated using VO₂ and RER values and subsequently normalized to body surface area (body mass^{-0.75}) to account for pronounced changes in body size associated with CR. Data were collected for three consecutive days, with the final 24 h period (6 am to 6 am) used for analysis.

In vitro muscle force. In vitro muscle force was measured in the fast-twitch *extensor digitorum longus* (EDL) and slow-twitch *soleus* muscles. After careful isolation, muscle tendons were tied with surgical sutures at each end and mounted on the 1200 A Isolated Muscle System (Aurora Scientific, Aurora, ON, Canada) in an organ bath containing 60 mL of Ringer solution (137 mM NaCl, 24 mM NaHCO₃, 11 mM Glucose, 5 mM KCl, 2 mM CaCl₂, 1 mM MgSO₄, 1 mM NaH₂PO₄) gassed with 95% O₂; 5% CO₂ at 30 °C. After defining optimal length, muscles were stimulated with 15 V pulses. Muscle force was recorded in response to 500 ms pulses of 10–250 Hz. Muscle fatigue was assessed by 6 min of repeated tetanic stimulations at 200 Hz for EDL and 120 Hz for SOL, respectively, separated by 8 s.

Immunostaining of muscle cross-sections. Muscles were mounted at resting length in optimal cutting temperature medium (O.C.T, Tissue-Tek) and snap-frozen in thawing isopentane for ~1 min before transfer to liquid nitrogen and storage at -80 °C. Muscle sections (10 μ m) were cut from the mid belly at -20 °C on a cryostat (Leica, CM1950), collected on SuperFrost Plus (VWR) adhesion slides and stored at -80 °C. Sections from each experimental condition were always mounted on the same slide to ensure accurate comparisons. For fiber typing, sections were blocked and permeabilized in PBS containing 10% goat serum and 0.4% triton X-100 for 30 min before being incubated for 2 h at RT in a primary antibody solution containing BA-D5, SC-71, BF-F3 which were developed by Professor Stefano Schiaffino and obtained from the Developmental Studies Hybridoma Bank developed under the auspices of the National Institute of Child Health and Human Development and maintained by the University of Iowa Department of Biology as well as laminin (#11575; Abcam) and 10% goat serum. After incubation in primary antibodies, sections were washed 4 \times 10 min in PBS and then incubated in a secondary antibody solution containing DyLight 405 (#115-475-207, Jackson), Alexa568 (#A-21124, Invitrogen), Alexa488 (#A-21042, Invitrogen), Alexa647 (#711-605-152, Jackson) and 10% goat serum. Sections were then washed 4 \times 10 min in PBS and mounted with ProLong™ Gold antifade (Invitrogen). Muscle sections were imaged at the Biozentrum Imaging Core Facility with an Axio Scan.Z1 Slide Scanner (Zeiss) equipped with appropriate band-pass filters. Fiji macros were developed in-house to allow an automated analysis of muscle fiber types (based on intensity thresholds) and muscle cross-sectional area (i.e., minimal Feret's diameter; based on cell segmentation)³¹. All macros and scripts used in this study are available upon request. For p62 staining, TA sections were thawed for 10 min at RT, fixed in 4% PFA for 6 min, neutralized in 0.1 M Glycine (pH7.4) at RT for 2 \times 15 min and then blocked at RT for 1.5 h in blocking solution containing 3% IgG free Bovine Serum Albumin (BSA), 1% Fab anti-mouse IgG (Jackson) and 0.25% Triton-X. Slides were then incubated in primary antibody solution containing p62 (GP62-C, 1:300), laminin (ab11576, Jackson 1:300) and 3%

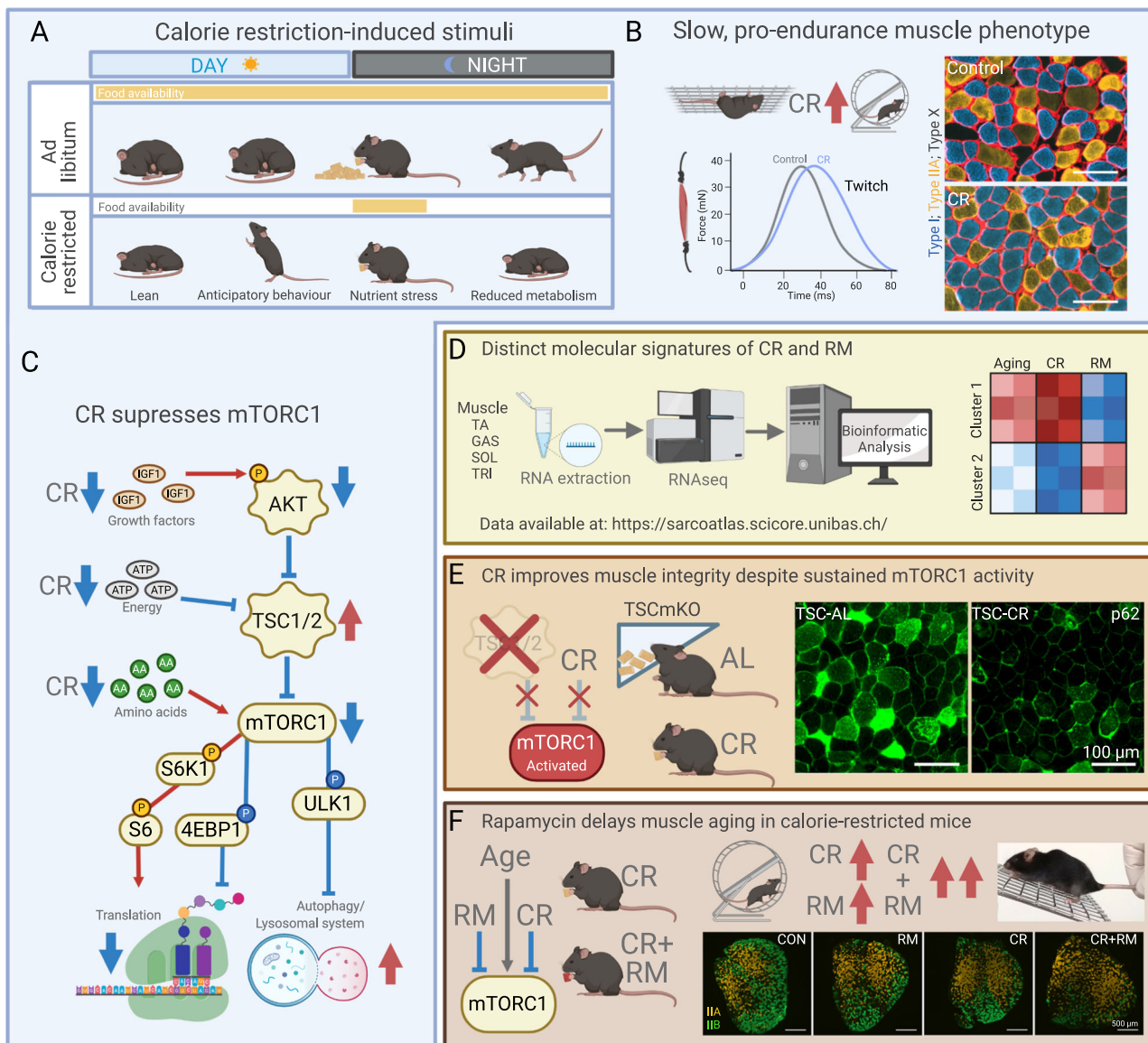


Fig. 8 Is rapamycin a calorie restriction mimetic? **A** Calorie restriction (CR) induces broad changes in activity (e.g., anticipatory behavior), metabolism (e.g., reduced metabolic rate), nutrition (e.g., nutrient stress and temporally compressed food intake) and body composition (e.g., reduced body mass and lean phenotype). **B** Long-term CR promotes a slow, pro-endurance muscle phenotype including improved endurance performance, slower contraction speeds and a fast-to-slow fiber type shift, particularly in the depicted soleus muscle. **C** CR suppresses mTORC1 activity by lowering the availability of its positive regulators, including growth factors, energy, and amino acids, leading to reduced translation and increased autophagy. **D** Despite both RM and CR suppressing mTORC1 activity, long-term treatments exert distinct and often opposing molecular signatures in aging skeletal muscle. **E** CR improves muscle quality in TSCmKO mice, which display sustained, nutrient-insensitive mTORC1 activity and a premature sarcopenic phenotype, indicating that muscle mTORC1 suppression is not required for CR-induced benefits. **F** While CR and RM both improve whole-body muscle function and promote a fast-to-slow fiber type switch, the effects are frequently additive in calorie-restricted mice treated with RM. Together, these data demonstrate that RM is not a CR mimetic, but could rather be an adjunct therapy for CR-like interventions. Figure created with BioRender.com.

BSA overnight at 4 °C. The next day, slides were washed 3 × 10 min in PBS and incubated in secondary antibody solution containing DaGP Cy3 (706-165-148; Jackson; 1:500) and GaRt 488 (112-545-003, Jackson; 1:500) for 1.5 h at RT. Afterwards, sections were washed 2 × 10 min in PBS and mounted with Vectashield DAPI (Vector Laboratories).

Protein extraction and western blot analysis. For TSC-CR studies, TA and GAS muscles were snap-frozen, pulverized in liquid nitrogen and lysed in RIPA buffer before sonication and 2 h incubation at 4 °C. Lysates were then centrifuged at 16,000 g for 30 min at 4 °C to remove insoluble material. Protein concentration was measured (BCA assay) and normalized with RIPA buffer before being heated for 5 min at 95 °C in Laemmli buffer (0.1 M Tris-HCl pH 6.8, 10% Glycerol, 2% SDS, 0.04% Bromophenolblue, 1% β-mercaptoethanol). Proteins were separated on 4–12% Bis-Tris protein gels (NuPAGE, Life Technologies) and transferred onto nitrocellulose membranes. Membranes were blocked for 1 h at RT in 3% BSA in

TBS containing 0.1% Tween20 and incubated overnight with primary antibodies in blocking solution at 4 °C. The next day, membranes were washed 3 × 10 min in TBS before incubation in secondary horseradish peroxidase-conjugated antibodies, diluted in blocking solution. Membranes were then washed 3 × 10 min in TBS before immunoreactivity was visualized using the KLP LumiGlo Chemiluminescence Substrate Kit (Seracare) with a Fusion Fx machine (Vilber). Protein abundance was quantified using FusionCapt Advance (Vilber) as mean grey value minus background and then normalized to a housekeeping protein. Western blots for all proteins were performed on TA muscle. For key proteins (phospho and total mTOR, S6, 4EBP1 and Akt, as well as p62 and LC3B), western blots were also performed on GAS muscle. Results in both muscles were comparable and were subsequently averaged for each mouse for further analysis. All primary antibodies were from Cell Signaling Technology: p^{S2448}mTOR (#2971), mTOR (#2972), p^{S240/244}S6 (#5364), p^{S235/236}S6 (#2211), S6 (#2217), p^{S65}4EBP1 (#9451), 4EBP1 (#9452), LC3B (#2775), p^{S757}ULK (#6888), ULK (#8054), Beclin1 (#3495), Bnip3 (#3769),

p^{T246}PRAS40 (#2997), PRAS40 (#2610), p^{S473}Akt (#4058), Akt (#9272) and BiP (#3177) at a dilution of 1:1000, except ATF4 (sc-200, Santa Cruz, 1:1000), FGF21 (AF3057, 1:500), α -actinin (A7732, Sigma, 1:5000) and p62 (GP62-C, Pro-Gen, 1:1000).

Plasma cytokines. Plasma cytokines were measured with a V-PLEX Pro-inflammatory Panel 1 Mouse Kit (Meso Scale Discovery) customized for five analytes (INF- γ , IL-1 β , IL-6, IL-10, TNF- α) using a twofold dilution and following the manufacturer's instructions.

RT-qPCR. Snap frozen gastrocnemius muscles were pulverized and lysed in RLT buffer (Qiagen). RNA was extracted using the RNeasy[®] Mini Kit (Qiagen), with Proteinase K and DNase treatment, according to the supplier's instructions. RNA purity was determined using a Nanodrop ONEC (Thermo Scientific). cDNA was generated with the iScript[™] cDNA Synthesis Kit (Bio-Rad) using 500 ng of extracted RNA according to supplier's manual. cDNA samples were stored at -20 °C. RT-qPCR was performed in duplicate with the LightCycler 480 (Roche Diagnostics) instrument using LightCycler 384-well plates with sealing foil (Roche). The reaction volume of 10 μ l contained, FastStart Essential DNA Green Master Mix (2X, Roche), forward and reverse primers and cDNA template (1:5 diluted). Primers were designed using Genious[®]10 software⁶⁶ and specificity confirmed by the Basic Local Alignment Search Tool (BLAST)⁶⁷. Potential hairpin formation, complementarity and self-annealing sites were verified to be negative by OligoCalc⁶⁸. The amplification of a single PCR product was confirmed with a melting-point dissociation curve and raw quantification cycle (Cq) values were calculated by a LightCycler 480. Data were analyzed using the comparative Cq method ($2^{-\Delta\Delta Cq}$). Raw Cq values of target genes were normalized to Cq values of a housekeeping gene (β -actin), which was stable between conditions, and then further normalized to the control group for ease of visualization. Primers used are as follows:

Map1lc3a: Fwd-GTTGGATGTGTCTGTCTCGTCAC; Rev-CTACGTGATTA TTTCCGTGTTGCT
Atg7: Fwd-TGCAGTTCGCCCTTTAAT; Rev-CAGGCGGTACTCGTTC AACT
Bnip3: Fwd-TTCCACTAGCACCTTCTGATGA; Rev-GAACACCCGATTTAC AGAACAA
Gabarapl1: Fwd-CATCGTGGAGAAGGCTCCTA; Rev-ATACAGCTGGCCCA TGGTAG
Sqstm1: Fwd-TACTCGAACGACACAAGGGA; Rev-GACTCAGCTGTAGGG CAAGG
Ctst: Fwd-GTGGACTGTTCTCACGCTCA; Rev-TCCGTCCTTCGCTTCA TAGG
Trib3: Fwd-GGACAAGATGCGAGCCACAT; Rev-CCACAGCAGGTGAC AAGTCT
Xbp1: Fwd-TGGCCGGTCTGCTGAGTCCG; Rev-GTCCATGGGAAGATG TTCTGG
Keap1: Fwd-GGCAGGACCAGTTGAACAGT; Rev-GGGTCACTCACTCCA GGTA
Gsta1: Fwd-CCAGAGCCATTCTCAACTA; Rev-TGCCCAATCATTTTCAG TCAG

RNA extraction for aging-calorie restriction data sets. For the aging-CR-RM data set, RNA extraction was performed as previously described in detail¹³. Briefly, TA, TRI, GAS and SOL muscles from 6 mice per group were pulverized and lysed in RLT buffer (Qiagen) and treated with proteinase K (Qiagen) and DNase. RNA was extracted with an iColumn 24 (AccuBioMed) with an AccuPure Tissue RNA Mini Kit (AccuBioMed). RNA purity and integrity was examined with a Bioanalyser (Agilent). RNA concentration was determined with a Quant-iT[™] RiboGreen[™] RNA assay kit and Qubit fluorometer (Invitrogen). Libraries were prepared with TruSeq Stranded mRNA HT Sample Prep Kit. Stranded, paired-end sequencing with 101 base pair read length was performed on an Illumina HiSeq2500 platform. A single outlier in the 30mCON SOL group was identified and removed from further analysis based on a clear technical error.

Statistical analysis. All values are expressed as mean \pm SEM unless stated otherwise. Data were tested for normality and homogeneity of variance using a Shapiro-Wilk and Levene's test, respectively. Data were analysed in GraphPad Prism 8. Student's *t* tests were used for pairwise comparisons, while one-way analyses of variance (ANOVAs) with Fisher's LSD post hoc tests were used to compare between three groups, so long as the ANOVA reached statistical significance. Two-way ANOVAs or two-way repeated measures ANOVAs for multiple recordings over time, with Sidak or Tukey's post hoc tests were used to compare between groups with two independent variables. Both significant differences ($P < 0.05$) and trends ($P < 0.1$) are reported where appropriate.

RNA-Seq data processing. Paired-end RNA-Seq reads were subjected to 3' adapter (mate 1 5'-AGATCGGAAGAGCACACGTG-3', mate 2 5'-AGATCG GAAGAGCGTCGTGT-3') and poly(A)/poly(T) trimming using Cutadapt v1.9.1⁶⁹. Reads shorter than 30 nucleotides were discarded. As the reference

transcriptome, we considered sequences of protein-coding transcripts with support level 1-3 based on the genome assembly GRCh38 (release 92) for mouse and corresponding transcript annotations from Ensembl database⁷⁰. The kallisto v0.43.1 software was used to assign filtered reads to mouse transcriptome⁷¹. The default options of kallisto were utilized for building the transcriptome index. For aligning stranded RNA-Seq reads, where mates 1 and 2 originated from antisense and sense strands, respectively, the option "--rf-stranded" was used. The option "--pseudobam" was used to save kallisto pseudoalignments to a BAM file.

Mapped reads were then assigned to transcripts in a weighted manner: if a read was uniquely mapped to a transcript, then the transcript's read count was incremented by 1; if a read was mapped to *n* different transcripts, each transcript's read count was incremented by 1/*n*. Trimming 3' adapters and poly(A)/poly(T) stretches, indexing reference transcriptomes, mapping the RNA-Seq reads to transcripts and counting reads assigned to individual transcripts were performed with a Snakemake framework⁷².

The expression of each transcript t_i was then estimated in units of transcripts per million (TPM) by dividing the read count c_i corresponding to the transcript by the transcript length l_i and normalizing to the library size:

$$t_i = \frac{c_i}{l_i} \cdot \frac{10^6}{\sum_{j=1}^n \frac{c_j}{l_j}} \quad (1)$$

The expression level of a gene was calculated as the sum of normalized expression levels of transcripts associated with the gene. For every gene, read counts of transcripts associated with this gene were also summed up.

Calculating log-fold changes in the gene expression across conditions. Calculating log-fold changes in the gene expression across conditions was performed with EdgeR available through the R/Bioconductor package⁷³. A gene was included in the analysis only if it had at least 1 count per million (CPM) in the number of samples corresponding to the minimum number of replicates of the same condition across conditions. Obtained log-fold changes were subjected to the hierarchical clustering based on Euclidean distance.

Aligning gene expression with principal components. The gene expression matrix with samples as columns and log₂-transformed gene expression in TPM units as rows was mean centered to make the data comparable both across samples and genes. The centered gene expression matrix was further subjected to the principal component analysis (PCA). First four principal components, PC1, PC2, PC3 and PC4, were defined for each data subset, respectively. Then for each data subset we quantified how much individual genes contributed to the corresponding principal component¹³. Shortly, we represented genes in the multi-dimensional sample space, localized principal components and calculated projections of vectors associated with genes on principal components and correlations between gene vectors and principal components. We considered a projection of the gene vector on PC significant if its absolute *z*-score value was ≥ 1.96 . The correlation between a gene vector and PC was considered as significant if the absolute value was ≥ 0.4 .

Hierarchical clustering. Hierarchical clustering of genes was based on Euclidean distance between changes in the gene expression in notified conditions (see Fig. 3E).

Gene ontology analysis. To annotate genes aligned with PCs, we performed the gene ontology (GO) analysis using Database for Annotation, Visualization and Integrated Discovery (DAVID)⁷⁴ through the R/Bioconductor package called "RDAVIDWebService"⁷⁵. "GOTERM_BP_DIRECT", "GOTERM_MF_DIRECT", and "GOTERM_CC_DIRECT" categories were used for gene annotation. Background genes for calculating enrichment statistics consisted of all genes expressed in muscle samples (see the section "Aligning gene expression with principal components"). GO terms with a *p* value < 0.01 were considered significantly enriched.

Shiny application. To make CR high-throughput data set and data analysis tools available for the research community, we included them in the previously developed interactive web application "SarcoAtlas" based on the R package Shiny (version 0.14.2, <https://cran.r-project.org/web/packages/shiny/index.html>). The application supports gene expression plotting, differential expression analysis, principal component analysis and aligning gene expression with principal components. Moreover, the application can submit genes resulting from the analysis to STRING⁷⁶ to further investigate protein-protein interactions and perform GO analysis. The application can be accessed through the following link: <https://sarcoatlas.scicore.unibas.ch/13,14>.

Reporting summary. Further information on research design is available in the Nature Research Reporting Summary linked to this article.

Data availability

The data supporting the findings from this study are available within the manuscript and its supplementary information. RNA-Seq data set on four muscles (GAS, TA, TRI, and

SOL) from six 30-month-old calorie-restricted mice was deposited to Gene Expression Omnibus (GEO)⁷⁷ under the accession number [GSE171322](https://www.ncbi.nlm.nih.gov/geo/query/acc.cgi?acc=GSE171322). RNA-Seq data describing profiles of four muscles (GAS, TA, TRI, and SOL) of 10-month-old, 30-month-old, and 30-month-old mice treated with rapamycin were previously published¹³ and are available at GEO under the accession number [GSE139204](https://www.ncbi.nlm.nih.gov/geo/query/acc.cgi?acc=GSE139204). These data are also accessible using the web-based application, SarcoAtlas (<https://sarcoatlas.scicore.unibas.ch/>). Source data are provided with this paper.

Code availability

Code for RNA-Seq analysis is available upon request from the corresponding author N.M. Code for fiber size analysis is available from the corresponding author D.H.

Received: 19 May 2021; Accepted: 28 March 2022;

Published online: 19 April 2022

References

- Most, J., Tosti, V., Redman, L. M. & Fontana, L. Calorie restriction in humans: an update. *Ageing Res. Rev.* **39**, 36–45 (2017).
- McCracken, A. W., Adams, G., Hartshorne, L., Tatar, M. & Simons, M. J. P. The hidden costs of dietary restriction: implications for its evolutionary and mechanistic origins. *Sci. Adv.* **6**, eaay3047 (2020).
- Fontana, L. & Partridge, L. Promoting health and longevity through diet: from model organisms to humans. *Cell* **161**, 106–118 (2015).
- Powers, R. W. 3rd, Kaerberlein, M., Caldwell, S. D., Kennedy, B. K. & Fields, S. Extension of chronological life span in yeast by decreased TOR pathway signaling. *Genes Dev.* **20**, 174–184 (2006).
- Bjedov, I. et al. Mechanisms of life span extension by rapamycin in the fruit fly *Drosophila melanogaster*. *Cell Metab.* **11**, 35–46 (2010).
- Robida-Stubbs, S. et al. TOR signaling and rapamycin influence longevity by regulating SKN-1/Nrf and DAF-16/FoxO. *Cell Metab.* **15**, 713–724 (2012).
- Harrison, D. E. et al. Rapamycin fed late in life extends lifespan in genetically heterogeneous mice. *Nature* **460**, 392–395 (2009).
- Unnikrishnan, A., Kurup, K., Salmon, A. B. & Richardson, A. Is rapamycin a dietary restriction mimetic? *J. Gerontol. A Biol. Sci. Med. Sci.* **75**, 4–13 (2020).
- WHO. *Decade of Healthy Ageing: Baseline Report* (World Health Organization, Geneva, 2020).
- Bodine, S. C. et al. Akt/mTOR pathway is a crucial regulator of skeletal muscle hypertrophy and can prevent muscle atrophy in vivo. *Nat. Cell Biol.* **3**, 1014–1019 (2001).
- Moro, T., Ebert, S. M., Adams, C. M. & Rasmussen, B. B. Amino acid sensing in skeletal muscle. *Trends Endocrinol. Metab.* **27**, 796–806 (2016).
- Stallone, G., Infante, B., Prisciandaro, C. & Grandaliano, G. mTOR and aging: an old fashioned dress. *Int. J. Mol. Sci.* <https://doi.org/10.3390/ijms20112774> (2019).
- Ham, D. J. et al. The neuromuscular junction is a focal point of mTORC1 signaling in sarcopenia. *Nat. Commun.* **11**, 4510 (2020).
- Borsch, A. et al. Molecular and phenotypic analysis of rodent models reveals conserved and species-specific modulators of human sarcopenia. *Commun. Biol.* **4**, 194 (2021).
- Valdez, G. et al. Attenuation of age-related changes in mouse neuromuscular synapses by caloric restriction and exercise. *Proc. Natl Acad. Sci. USA* **107**, 14863–14868 (2010).
- Jang, Y. C. et al. Dietary restriction attenuates age-associated muscle atrophy by lowering oxidative stress in mice even in complete absence of CuZnSOD. *Ageing Cell* **11**, 770–782 (2012).
- van Norren, K. et al. Behavioural changes are a major contributing factor in the reduction of sarcopenia in caloric-restricted ageing mice. *J. Cachexia Sarcopenia Muscle* **6**, 253–268 (2015).
- Margolis, L. M. et al. Prolonged calorie restriction downregulates skeletal muscle mTORC1 signaling independent of dietary protein intake and associated microRNA expression. *Front. Physiol.* **7**, 445 (2016).
- Fok, W. C. et al. Short-term treatment with rapamycin and dietary restriction have overlapping and distinctive effects in young mice. *J. Gerontol. A Biol. Sci. Med. Sci.* **68**, 108–116 (2013).
- Houde, V. P. et al. Chronic rapamycin treatment causes glucose intolerance and hyperlipidemia by upregulating hepatic gluconeogenesis and impairing lipid deposition in adipose tissue. *Diabetes* **59**, 1338–1348 (2010).
- Fok, W. C. et al. Combined treatment of rapamycin and dietary restriction has a larger effect on the transcriptome and metabolome of liver. *Ageing Cell* **13**, 311–319 (2014).
- Karunadharma, P. P. et al. Subacute calorie restriction and rapamycin discordantly alter mouse liver proteome homeostasis and reverse aging effects. *Ageing Cell* **14**, 547–557 (2015).
- Mitchell, S. E. et al. The effects of graded levels of calorie restriction: I. impact of short term calorie and protein restriction on body composition in the C57BL/6 mouse. *Oncotarget* **6**, 15902–15930 (2015).
- Mitchell, S. E. et al. The effects of graded levels of calorie restriction: III. Impact of short term calorie and protein restriction on mean daily body temperature and torpor use in the C57BL/6 mouse. *Oncotarget* **6**, 18314–18337 (2015).
- Reynolds, T. H. et al. The impact of age and sex on body composition and glucose sensitivity in C57BL/6J mice. *Physiol. Rep.* **7**, e13995 (2019).
- Guridi, M. et al. Activation of mTORC1 in skeletal muscle regulates whole-body metabolism through FGF21. *Sci. Signal.* **8**, ra113 (2015).
- Joseph, G. A. et al. Partial inhibition of mTORC1 in aged rats counteracts the decline in muscle mass and reverses molecular signaling associated with sarcopenia. *Mol. Cell. Biol.* <https://doi.org/10.1128/MCB.00141-19> (2019).
- Baar, E. L., Carbajal, K. A., Ong, I. M. & Lamming, D. W. Sex- and tissue-specific changes in mTOR signaling with age in C57BL/6J mice. *Ageing Cell* **15**, 155–166 (2016).
- Tang, H. et al. mTORC1 underlies age-related muscle fiber damage and loss by inducing oxidative stress and catabolism. *Ageing Cell* **18**, e12943 (2019).
- Conti, B. Considerations on temperature, longevity and aging. *Cell. Mol. Life Sci.* **65**, 1626–1630 (2008).
- Delezie, J. et al. BDNF is a mediator of glycolytic fiber-type specification in mouse skeletal muscle. *Proc. Natl Acad. Sci. USA* **116**, 16111–16120 (2019).
- Blagosklonny, M. V. Calorie restriction: decelerating mTOR-driven aging from cells to organisms (including humans). *Cell Cycle* **9**, 683–688 (2010).
- Castets, P. et al. Sustained activation of mTORC1 in skeletal muscle inhibits constitutive and starvation-induced autophagy and causes a severe, late-onset myopathy. *Cell Metab.* **17**, 731–744 (2013).
- White, Z., White, R. B., McMahon, C., Grounds, M. D. & Shavlakadze, T. High mTORC1 signaling is maintained, while protein degradation pathways are perturbed in old murine skeletal muscles in the fasted state. *Int. J. Biochem. Cell Biol.* **78**, 10–21 (2016).
- Um, S. H. et al. Absence of S6K1 protects against age- and diet-induced obesity while enhancing insulin sensitivity. *Nature* **431**, 200–205 (2004).
- Lee, A. H., Iwakoshi, N. N. & Glimcher, L. H. XBP-1 regulates a subset of endoplasmic reticulum resident chaperone genes in the unfolded protein response. *Mol. Cell. Biol.* **23**, 7448–7459 (2003).
- Dodson, M., Redmann, M., Rajasekaran, N. S., Darley-Usmar, V. & Zhang, J. KEAP1-NRF2 signalling and autophagy in protection against oxidative and reductive proteotoxicity. *Biochem. J.* **469**, 347–355 (2015).
- Goodpaster, B. H. & Sparks, L. M. Metabolic flexibility in health and disease. *Cell Metab.* **25**, 1027–1036 (2017).
- Kirkwood, T. B. & Shanley, D. P. Food restriction, evolution and ageing. *Mech. Ageing Dev.* **126**, 1011–1016 (2005).
- Shanley, D. P. & Kirkwood, T. B. Calorie restriction and aging: a life-history analysis. *Evolution* **54**, 740–750 (2000).
- Lee, C. K., Klopp, R. G., Weindruch, R. & Prolla, T. A. Gene expression profile of aging and its retardation by caloric restriction. *Science* **285**, 1390–1393 (1999).
- Kirkwood, T. B. & Austad, S. N. Why do we age? *Nature* **408**, 233–238 (2000).
- Boldrin, L. et al. The effect of calorie restriction on mouse skeletal muscle is sex, strain and time-dependent. *Sci. Rep.* **7**, 5160 (2017).
- Giller, K. et al. Beneficial effects of a 6-month dietary restriction are time-dependently abolished within 2 weeks or 6 months of refeeding-genome-wide transcriptome analysis in mouse liver. *Free Radic. Biol. Med.* **61**, 170–178 (2013).
- Most, J. & Redman, L. M. Impact of calorie restriction on energy metabolism in humans. *Exp. Gerontol.* **133**, 110875 (2020).
- Sohal, R. S. & Forster, M. J. Caloric restriction and the aging process: a critique. *Free Radic. Biol. Med.* **73**, 366–382 (2014).
- Redman, L. M. et al. Metabolic slowing and reduced oxidative damage with sustained caloric restriction support the rate of living and oxidative damage theories of aging. *Cell Metab.* **27**, 805–815.e804 (2018).
- Sinclair, D. A. Toward a unified theory of caloric restriction and longevity regulation. *Mech. Ageing Dev.* **126**, 987–1002 (2005).
- Gordon, P. M. et al. Resistance exercise training influences skeletal muscle immune activation: a microarray analysis. *J. Appl. Physiol.* **112**, 443–453 (2012).
- Lecker, S. H. et al. Multiple types of skeletal muscle atrophy involve a common program of changes in gene expression. *FASEB J.* **18**, 39–51 (2004).
- Ibeunjo, C. et al. Genomic and proteomic profiling reveals reduced mitochondrial function and disruption of the neuromuscular junction driving rat sarcopenia. *Mol. Cell. Biol.* **33**, 194–212 (2013).
- Zhou, J., Liao, Z., Chen, J., Zhao, K. & Xiao, Q. Integrated study on comparative transcriptome and skeletal muscle function in aged rats. *Mech. Ageing Dev.* **169**, 32–39 (2018).

53. Ewald, C. Y., Landis, J. N., Porter Abate, J., Murphy, C. T. & Blackwell, T. K. Dauer-independent insulin/IGF-1-signalling implicates collagen remodelling in longevity. *Nature* **519**, 97–101 (2015).
54. Chen, Y. L. et al. Adiponectin receptor PAQR-2 signaling senses low temperature to promote *C. elegans* longevity by regulating autophagy. *Nat. Commun.* **10**, 2602 (2019).
55. Schumacher, B. et al. Delayed and accelerated aging share common longevity assurance mechanisms. *PLoS Genet.* **4**, e1000161 (2008).
56. Nilsson, M. I. et al. Lifelong aerobic exercise protects against inflammaging and cancer. *PLoS ONE* **14**, e0210863 (2019).
57. White, Z. et al. Voluntary resistance wheel exercise from mid-life prevents sarcopenia and increases markers of mitochondrial function and autophagy in muscles of old male and female C57BL/6J mice. *Skelet. Muscle* **6**, 45 (2016).
58. Kim, J. H., Kwak, H. B., Leeuwenburgh, C. & Lawler, J. M. Lifelong exercise and mild (8%) caloric restriction attenuate age-induced alterations in plantaris muscle morphology, oxidative stress and IGF-1 in the Fischer-344 rat. *Exp. Gerontol.* **43**, 317–329 (2008).
59. Mitchell, S. E. et al. The effects of graded levels of calorie restriction: V. Impact of short term calorie and protein restriction on physical activity in the C57BL/6 mouse. *Oncotarget* **7**, 19147–19170 (2016).
60. Miller, R. A. et al. Rapamycin-mediated lifespan increase in mice is dose and sex dependent and metabolically distinct from dietary restriction. *Aging Cell* **13**, 468–477 (2014).
61. Mitchell, S. J. et al. Effects of sex, strain, and energy intake on hallmarks of aging in mice. *Cell Metab.* **23**, 1093–1112 (2016).
62. Kane, A. E., Sinclair, D. A., Mitchell, J. R. & Mitchell, S. J. Sex differences in the response to dietary restriction in rodents. *Curr. Opin. Physiol.* **6**, 28–34 (2018).
63. Tulsian, R., Velingkaar, N. & Kondratov, R. Caloric restriction effects on liver mTOR signaling are time-of-day dependent. *Aging* **10**, 1640–1648 (2018).
64. Lamming, D. W. et al. Rapamycin-induced insulin resistance is mediated by mTORC2 loss and uncoupled from longevity. *Science* **335**, 1638–1643 (2012).
65. Kwiatkowski, D. J. et al. A mouse model of TSC1 reveals sex-dependent lethality from liver hemangiomas, and up-regulation of p70S6 kinase activity in Tsc1 null cells. *Hum. Mol. Genet.* **11**, 525–534 (2002).
66. Kearse, M. et al. Geneious basic: an integrated and extendable desktop software platform for the organization and analysis of sequence data. *Bioinformatics* **28**, 1647–1649 (2012).
67. Altschul, S. F., Gish, W., Miller, W., Myers, E. W. & Lipman, D. J. Basic local alignment search tool. *J. Mol. Biol.* **215**, 403–410 (1990).
68. Kibbe, W. A. OligoCalc: an online oligonucleotide properties calculator. *Nucleic Acids Res.* **35**, W43–W46 (2007).
69. Martin, M. Cutadapt removes adapter sequences from high-throughput sequencing reads. *EMBnet J.* **17**, 10–12 (2011).
70. Hubbard, T. et al. The Ensembl genome database project. *Nucleic Acids Res.* **30**, 38–41 (2002).
71. Bray, N. L., Pimentel, H., Melsted, P. & Pachter, L. Near-optimal probabilistic RNA-seq quantification. *Nat. Biotechnol.* **34**, 525–527 (2016).
72. Koster, J. & Rahmann, S. Snakemake—a scalable bioinformatics workflow engine. *Bioinformatics* **34**, 3600 (2018).
73. Durinck, S., Spellman, P. T., Birney, E. & Huber, W. Mapping identifiers for the integration of genomic datasets with the R/Bioconductor package biomaRt. *Nat. Protoc.* **4**, 1184–1191 (2009).
74. Huang da, W., Sherman, B. T. & Lempicki, R. A. Systematic and integrative analysis of large gene lists using DAVID bioinformatics resources. *Nat. Protoc.* **4**, 44–57 (2009).
75. Fresno, C. & Fernandez, E. A. RDAVIDWebService: a versatile R interface to DAVID. *Bioinformatics* **29**, 2810–2811 (2013).
76. Snel, B., Lehmann, G., Bork, P. & Huynen, M. A. STRING: a web-server to retrieve and display the repeatedly occurring neighbourhood of a gene. *Nucleic Acids Res.* **28**, 3442–3444 (2000).
77. Barrett, T. et al. NCBI GEO: archive for high-throughput functional genomic data. *Nucleic Acids Res.* **37**, D885–D890 (2009).

Acknowledgements

We gratefully acknowledge Dr. Mikhail Pachkov for help with data processing, Dr. Alexander Kanitz for testing, Pablo Escobar López for publishing SarcoAtlas, and Dr. Erik van Nimwegen for fruitful discussions about data analysis. We also acknowledge the support of the University of Basel's Quantitative Genomics Facility, in particular Philippe Demougin for assistance with mRNA-Seq sample preparation; the Image Core Facility, in particular Kai Schleicher; and the scientific computing center, sciCORE (<http://scicore.unibas.ch/>), where calculations were performed. This work was financially supported by the Cantons of Basel-Stadt and Basel-Landschaft, a jubiläumstiftung from Swiss Life awarded to NM, and a Sinergia grant (CRSII3_160760) from the Swiss National Science Foundation awarded to M.A.R., M.Z., and C.H.

Author contributions

Conceptualization: D.J.H., N.M., M.A.R., M.Z., A.B., L.A.T.; methodology: D.J.H., N.M., K.C., S.L., L.A.T., A.B.; investigation: D.J.H., N.M., K.C., S.L., A.B.L., A.S.H., R.F., M.T., J.D., L.A.T., D.B.; data curation and formal analysis: A.B., D.J.H.; statistical analysis: D.J.H., A.B.; software: A.B.; visualization: D.J.H., A.B.; supervision: M.A.R., M.Z.; writing original draft: D.J.H., A.B., M.A.R.; writing review and editing: D.J.H., M.A.R., N.M., A.B., M.Z., L.T.; funding acquisition: M.A.R., M.Z., N.M., C.H., M.S.

Competing interests

The authors declare no competing interests.

Additional information

Supplementary information The online version contains supplementary material available at <https://doi.org/10.1038/s41467-022-29714-6>.

Correspondence and requests for materials should be addressed to Daniel J. Ham, Nitish Mittal or Markus A. Ruegg.

Peer review information *Nature Communications* thanks Mark Tarnopolsky, James White, and the other anonymous reviewer for their contribution to the peer review of this work.

Reprints and permission information is available at <http://www.nature.com/reprints>

Publisher's note Springer Nature remains neutral with regard to jurisdictional claims in published maps and institutional affiliations.



Open Access This article is licensed under a Creative Commons Attribution 4.0 International License, which permits use, sharing, adaptation, distribution and reproduction in any medium or format, as long as you give appropriate credit to the original author(s) and the source, provide a link to the Creative Commons license, and indicate if changes were made. The images or other third party material in this article are included in the article's Creative Commons license, unless indicated otherwise in a credit line to the material. If material is not included in the article's Creative Commons license and your intended use is not permitted by statutory regulation or exceeds the permitted use, you will need to obtain permission directly from the copyright holder. To view a copy of this license, visit <http://creativecommons.org/licenses/by/4.0/>.

© The Author(s) 2022